Neurobiology of Disease

Context-Specific Switch from Anti- to Pro-epileptogenic Function of the $P2Y_1$ Receptor in Experimental Epilepsy

Mariana Alves,[1] Laura De Diego Garcia,[1] Giorgia Conte,[1] Eva M. Jimenez-Mateos,[1,2] Beatrice D'Orsi,[1,3] Amaya Sanz-Rodriguez,[1] Jochen H.M. Prehn,[1,4] David C. Henshall,[1,4] and Tobias Engel[1,4]

[1]Department of Physiology & Medical Physics, Royal College of Surgeons in Ireland, Dublin 2, Ireland, [2]Discipline of Physiology, School of Medicine, Trinity College Ireland, University of Dublin, Dublin 2, Ireland, [3]Department of Biomedical Sciences, University of Padova, 35131 Padova, Italy, and [4]FutureNeuro Research Centre, RCSI, Dublin 2, Ireland

Extracellular ATP activates inflammatory responses to tissue injury. It is also implicated in establishing lasting network hyperexcitability in the brain by acting upon independent receptor systems. Whereas the fast-acting P2X channels have well-established roles driving neuroinflammation and increasing hyperexcitability, the slower-acting metabotropic P2Y receptors have received much less attention. Recent studies of $P2Y_1$ receptor function in seizures and epilepsy have produced contradictory results, suggesting that the role of this receptor during seizure pathology may be highly sensitive to context. Here, by using male mice, we demonstrate that the metabotropic $P2Y_1$ receptor mediates either proconvulsive or anticonvulsive responses, dependent on the time point of activation in relation to the induction of status epilepticus. $P2Y_1$ deficiency or a $P2Y_1$ antagonist (MRS2500) administered before a chemoconvulsant, exacerbates epileptiform activity, whereas a $P2Y_1$ agonist (MRS2365) administered at this time point is anticonvulsant. When these drugs are administered after the onset of status epilepticus, however, their effect on seizure severity is reversed, with the antagonist now anticonvulsant and the agonist proconvulsant. This result was consistent across two different mouse models of status epilepticus (intra-amygdala kainic acid and intraperitoneal pilocarpine). Pharmacologic $P2Y_1$ blockade during status epilepticus reduces also associated brain damage, delays the development of epilepsy and, when applied during epilepsy, suppresses spontaneous seizures, in mice. Our data show a context-specific role for $P2Y_1$ during seizure pathology and demonstrate that blocking $P2Y_1$ after status epilepticus and during epilepsy has potent anticonvulsive effects, suggesting that $P2Y_1$ may be a novel candidate for the treatment of drug-refractory status epilepticus and epilepsy.

Key words: animal models; $P2Y_1$ receptor; purinergic signaling; status epilepticus

Significance Statement

This is the first study to fully characterize the contribution of a metabotropic purinergic P2Y receptor during acute seizures and epilepsy. The findings suggest that targeting $P2Y_1$ may offer a potential novel treatment strategy for drug-refractory status epilepticus and epilepsy. Our data demonstrate a context-specific role of $P2Y_1$ activation during seizures, switching from a proconvulsive to an anticonvulsive role depending on physiopathological context. Thus, our study provides a possible explanation for seemingly conflicting results obtained between studies of different brain diseases where $P2Y_1$ targeting has been proposed as a potential treatment strategy and highlights that the timing of pharmacological interventions is of critical importance to the understanding of how receptors contribute to the generation of seizures and the development of epilepsy.

Introduction

Neuroinflammation is a critical tissue repair mechanism but also contributes to chronic hyperexcitability in the CNS. Consequently, targeting inflammatory processes has been proposed as a promising new treatment strategy for epilepsy (Vezzani and Vivi-

Received Jan. 11, 2019; revised March 21, 2019; accepted March 23, 2019.

Author contributions: M.A., L.D.D.G., G.C., E.M.J.-M., B.D., A.S.-R., and T.E. performed research; M.A., L.D.D.G., G.C., E.M.J.-M., B.D., and T.E. analyzed data; M.A., E.M.J.-M., J.H.M.P., D.C.H., and T.E. edited the paper; J.H.M.P. and D.C.H. contributed unpublished reagents/analytic tools; D.C.H. and T.E. designed research; T.E. wrote the first draft of the paper; T.E. wrote the paper.

This work was supported by Health Research Board HRA-POR-2015-1243 to T.E.; Science Foundation Ireland 13/SIRG/2098 and 17/CDA/4708 to T.E. and 13/SIRG/2114 to E.M.J.-M.; European Regional Development Fund and by FutureNeuro industry partners 16/RC/3948 to D.C.H. and 13/IA/1881 to J.H.M.P.; H2020 Marie Sklowdowksa-Curie Actions Individual Fellowship 796600 to L.D.D.G.; and European Union's Horizon 2020 research and innovation programme (Marie Sklowdowska-Curie Grant Agreement 766124) to T.E. We thank Dr. Heiko Duessmann for assistance with confocal microscopy.

The authors declare no competing financial interests.

Correspondence should be addressed to Tobias Engel at tengel@rcsi.ie.

https://doi.org/10.1523/JNEUROSCI.0089-19.2019

Copyright © 2019 the authors

ani, 2015). ATP, an important mediator of neuroinflammation, is ordinarily present at low extracellular micromolar concentrations in the CNS. Following injury, extracellular ATP concentrations increase to the millimolar range and activate purinergic P2 receptors (Dale and Frenguelli, 2009; Burnstock, 2013; Idzko et al., 2014). P2 receptors are subdivided into fast-acting ionotropic P2X channels and slower-acting metabotropic P2Y receptors, of which there are eight subtypes ($P2Y_{1,2,4,6,11,12,13,14}$) (Burnstock, 2013). Collectively, these receptors mediate diverse changes in the brain, including the coordination of inflammatory responses, thereby potentially contributing to increases in network hyperexcitability and epilepsy (Henshall and Engel, 2015). Whereas P2X receptors, in particular the P2X7 receptor subtype, have well-established roles in driving neuroinflammation and hyperexcitability (Beamer et al., 2017; Engel et al., 2016), P2Y receptors have received much less attention (Alves et al., 2018). Recent studies, however, suggest a prominent role for P2Y receptors in ictogenesis and possibly epileptogenesis (Alves et al., 2017). Among the P2Y receptor family, $P2Y_1$ has received most attention as a potential drug target for epilepsy (Alves et al., 2017; Simões et al., 2018; Nikolic et al., 2018).

The metabotropic $P2Y_1$ receptor is activated by the extracellular nucleotides adenosine diphosphate (ADP) and ATP. Under physiological conditions, $P2Y_1$ is expressed throughout the brain in neurons, astrocytes, and microglia (Burnstock and Knight, 2004). A role for $P2Y_1$ has been suggested in an array of different brain diseases, including acute insults to the CNS, such as traumatic brain injury (Choo et al., 2013; Talley Watts et al., 2013) and ischemia (Carmo et al., 2014; Fukumoto et al., 2018) and chronic diseases of the CNS, such as Alzheimer's disease (Delekate et al., 2014) and epilepsy (Alves et al., 2017). There have, however, been conflicting findings. $P2Y_1$ receptor activation significantly reduced postinjury symptoms following mechanical trauma in mice, including edema, neuronal swelling, and reactive gliosis (Talley Watts et al., 2013). In contrast, $P2Y_1$ receptor antagonism improved cognitive deficits and reduced damage in other models of traumatic brain injury (Choo et al., 2013; Carmo et al., 2014; Shinozaki et al., 2017). Similarly, contradictory results have also been obtained in models of ischemia, with some reports suggesting $P2Y_1$ contributing to brain damage (Kuboyama et al., 2011; Carmo et al., 2014) and others demonstrating $P2Y_1$ agonists being protective (Zheng et al., 2013; Fukumoto et al., 2018). Proconvulsive roles for $P2Y_1$ have been suggested by the observation that $P2Y_1$ receptor activation leads to enhanced Ca^{2+} signaling and astroglial activation in experimental kindling, a model of epileptogenesis (Álvarez-Ferradas et al., 2015). $P2Y_1$ has also been shown to regulate the release of different neurotransmitters in the brain, including glutamate, noradrenaline, and GABA, and to alter the sensitivity or availability of neurotransmitter receptors, including metabotropic glutamate receptor 1 (mGluR1), NMDA, gamma-aminobutyric acid ($GABA_A$), and P2X receptors (Guzman and Gerevich, 2016). A more recent study demonstrated that, although $P2Y_1$ antagonism had no effect on seizure severity, it significantly reduced seizure-induced neuronal loss in the hippocampus (Simoes et al., 2018). In contrast, another recent study demonstrated that antagonism of $P2Y_1$ suppressed excitatory synaptic activity in hippocampal slices from kainic acid (KA)-treated mice (Nikolic et al., 2018).

To identify the possible underlying cause of this apparent contrasting role for $P2Y_1$ in controlling excitability, we explored the consequences of targeting the receptor before and after triggering prolonged seizures (status epilepticus). Using a combination of genetic and pharmacological approaches, we demonstrate that the consequences of $P2Y_1$ activation diverge according to context, with a functional switch from anticonvulsive to proconvulsive effects when seizures occur. Consequently, we demonstrate that antagonism of this receptor can produce potent anticonvulsive effects, and we implicate a $P2Y_1$-driven microglia response as the likely mechanism through which $P2Y_1$ activation alters seizures and epileptogenesis.

Materials and Methods

Animal models. All animal experiments were performed in accordance with the principles of the European Communities Council Directive (2010/63/EU). Procedures were reviewed and approved by the Research Ethics Committee of the Royal College of Surgeons in Ireland (REC 1322 and REC 842) and the Irish Health Products Regulatory Authority (AE19127/P038 and AE19127/P001). All efforts were maximized to reduce the number of animals used in this study. Mice used in our experiments were 8- to 12-week-old male C57BL/6 mice, obtained from Harlan Laboratories and from the Biomedical Research Facility, Royal College of Surgeons in Ireland (Dublin, Ireland), or male *$P2Y_1$ Knock-out* (KO) mice, obtained from The Jackson Laboratory (009131-B6.129P2-P2ry1<tm1Bhk>/J). Animals were housed in a controlled biomedical facility on a 12 h light/dark cycle at 22 ± 1°C and humidity of 40%–60% with food and water provided *ad libitum*. Procedures to induce status epilepticus in mice were undertaken as described previously (Brennan et al., 2013). Before implantation of cannulas and electrodes, mice were anesthetized using isoflurane (5% induction, 1%–2% maintenance) and maintained normothermic by means of a feedback-controlled heat blanket (Harvard Apparatus). Next, mice were placed in a stereotaxic frame, and a midline scalp incision was performed to expose the skull. A guide cannula (coordinates from bregma; AP = −0.94 mm, lateral = −2.85 mm) and three electrodes for EEG recording (Bilaney Consultants), two above each hippocampus and one above the frontal cortex as reference, were fixed in place with dental cement. EEG was recorded using the Xltek recording system (Optima Medical).

To induce status epilepticus, KA (0.3 μg KA in 0.2 μl PBS) (Sigma-Aldrich) was administered into the basolateral amygdala (BLA) nucleus. Vehicle (Veh)-injected control animals received 0.2 μl of PBS. To reduce morbidity and mortality, mice were treated intraperitoneal (i.p) with the anticonvulsant lorazepam (6 mg/kg) (Wyetch) 40 min after KA or PBS injection. As described previously, all mice develop epilepsy after a short latency period of 3–5 d (Mouri et al., 2008).

In a subgroup of mice, status epilepticus was induced by an i.p injection of pilocarpine (Sigma-Aldrich) as described previously (Engel et al., 2013) at 340 mg/kg body weight, 20 min after injection of methylscopolamine (1 mg/kg) (Sigma-Aldrich). EEG was recorded as described above for 90 min following pilocarpine injection until administration of the anticonvulsant lorazepam (6 mg/kg, i.p.).

Drug administration. Mice were assigned randomly to receive either Veh or drug. Both $P2Y_1$ receptor antagonist MRS2500 (MRS25, 1 nmol) (Tocris Bioscience; 2159) and $P2Y_1$ agonist MRS2365 (MRS23, 0.3 and 1 nmol) (Tocris Bioscience; 2157) were delivered intracerebroventricularly (2 μl) (coordinates from bregma: AP = −0.4 mm; lateral = −0.95 mm) at different time points according to experimental setting. This included injections 15 min before KA treatment and 15 min, 60 min, 4 h, and 24 h after KA treatment. Ten days following the induction of status epilepticus, a subgroup of epileptic mice were also treated twice daily for 5 consecutive days with 1 nmol antagonist MRS25 (2 μl, i.c.v.). Drug doses were calculated according to EC_{50} value provided by supplier (MRS2500 EC_{50} = 0.95 nM; MRS2365 EC_{50} = 0.4 nM) or according to published data (MRS25) (Carmo et al., 2014; Simoes et al., 2018). Control mice were injected with 2 μl (i.c.v.) of the Veh solution (sterile H_2O). Minocycline (30 mg/kg, PBS) (Sigma-Aldrich, M9511) was delivered twice via intraperitoneal injection (200 μl) 4 and 24 h before intra-amygdala KA injection (Jimenez-Mateos et al., 2015).

EEG analysis during status epilepticus. To analyze EEG frequency, amplitude signal (power spectral density and EEG spectrogram of the EEG data) and seizure onset, EEG data were uploaded into Labchart7 software (AD Instruments). EEG total power (μV^2) is a function of EEG ampli-

tude over time and was analyzed by integrating frequency bands from 0 to 100 Hz. Power spectral density heat maps were generated within LabChart (spectral view), with the frequency domain filtered from 0–40 Hz and the amplitude domain filtered from 0–50 mV.

Long-term EEG telemetry recording. Spontaneous seizures during epilepsy were recorded using implantable telemetry devices (Data Science International, model F20-EET) (Jimenez-Pacheco et al., 2016), which allow for continuous EEG recording in freely-moving mice. These devices are implanted under the skin between the shoulders in the back of the animals and connected to cortical EEG electrodes. Once implanted, animals are placed in cages on top of receivers and devices are activated. EEG was recorded during a 14 or 20 d recording period following the induction of status epilepticus. EEG data were reviewed and seizures manually scored by an observer unaware of experimental treatment with epileptic seizures defined as high-frequency (>5 Hz) high-amplitude (>2 × baseline) polyspike discharges of >5 s duration.

RNA extraction and qPCR. RNA extraction was performed using the Trizol method, as described previously (Engel et al., 2017b). Quantity and quality of RNA were measured using a Nanodrop Spectrophotometer (Thermo Fisher Scientific). Samples with a 260/280 ratio between 1.8 and 2.2 were considered acceptable; 500 ng of total mRNA was used to produce cDNA by reverse transcription using SuperScript III reverse transcriptase enzyme (Invitrogen) primed with 50 pmol of random hexamers (Sigma-Aldrich). qPCR was performed using the QuantiTech SYBR Green kit (QIAGEN) and the LightCycler 1.5 (Roche Diagnostics). Each reaction tube contained 2 μl cDNA sample, 10 μl SYBR Green QuantiTech Reagent (QIAGEN), 1.25 μM primer pair (Sigma-Aldrich), and RNase free water (Invitrogen) to a final volume of 20 μl. Using LightCycler 1.5 software, data were analyzed and normalized to the expression of β-actin. Primers used (Sigma-Aldrich) were as follows: *GFAP* forward, AGAAAACCGCATCACCATTC, reverse, TCACATCACC ACGTCCTTGT; *Iba1* forward, TGGAGGGGATCAACAAGCAA, reverse, ACCCCAAGTTTCTCCAGCAT; *Cx3Cr1* forward, ACAGCCAG ACAAGAGGAGAC, reverse, CCGGAGTCAGTGAATGCATG; *ALDH1L1* forward, TCCAGGCCTAGTCACCAAAG, reverse, ATTGGGCAGAA TTCGCATCC; and *β-actin* forward: GGGTGTGATGGTGGGAATGG, reverse, GGTTGGCCTTAGGGTTCAGG).

Western blot analysis. Western blot analysis was performed as described previously (Engel et al., 2017b). Lysis buffer containing phosphatase and protease inhibitors was used to homogenize hippocampal tissue and extract protein, which was quantified using a Tecan plate reader at 560 nm; 30 μg of protein samples was loaded onto an acrylamide gel and separated by SDS-PAGE. After the electrophoresis process, proteins were transferred to a nitrocellulose membrane (GE Healthcare) and probed with the following primary antibodies: $P2Y_1$ (RRID:AB_2040070), $P2Y_2$ (RRID:AB_2040078), $P2Y_{12}$ (RRID:AB_2040074), $P2Y_{13}$ (RRID: AB_2040076, 1/200) (Alomone Labs), GFAP (RRID:AB_477035, 1/1000) (Sigma-Aldrich), Iba1 (RRID:AB_839504, 1/400) (Wako), GluR6/7 (RRID:AB_1587072, 1/1000) (Merck Millipore), synaptophysin (RRID:AB_2286949, 1/5000) (Abcam), and β-actin (catalog #A5441, 1:1000) (Sigma-Aldrich). Membranes were incubated with HRP-conjugated secondary antibodies (Jackson ImmunoResearch Laboratories), and protein bands were visualized using the LAS-4000 system (Fujifilm) with chemiluminescence (Merck Millipore) following analysis using Alpha-EaseFC4.0 software. Spot dense option was used to evaluate the optical density of each protein band. Protein quantity was normalized to the loading control (β-actin).

Synaptoneurosome preparation. Synaptoneurosomes of neuronal origin were prepared from mouse hippocampus as described with modifications (Jimenez-Pacheco et al., 2016). A pool of 2 hippocampi was homogenized in homogenization buffer (1 mM EDTA, 0.32 M sucrose, 1 mg/ml BSA, and 5 mM HEPES, pH 7.4) containing phosphatase and protease inhibitors, followed by centrifugation at 3000 × *g* for 10 min at 4°C. Supernatant (synaptoneurosomes and cytoplasm) was recovered and centrifuged at 14,000 × *g* for 12 min at 4°C. Pellet (synaptoneurosomes) was resuspended in 220 μl of Krebs-Ringer buffer (140 mM NaCl, 5 mM KCl, 5 mM glucose, 1 mM EDTA, and 10 mM HEPES, pH 7.4), and 180 μl of Percoll (45% v/v) was added to the tube followed by centrifugation at 14,000 × rpm for 2 min at 4°C. Synaptoneurosomes were recovered from the top layer with a sterile Pasteur pipette and resuspended in 1 ml of Krebs-Ringer buffer. Then, synaptoneurosomes were centrifuged at 14,000 × *g* for 30 s at 4°C and pellet resuspended in the same lysis buffer used for protein extraction containing phosphatase and protease inhibitors. Synaptoneurosome protein quantification was performed using a Tecan plate reader at 560 nm and samples analyzed via Western blotting.

Cytokine measurement in brain tissue. Interleukin-1β (IL-1β) and TNF-α levels in the hippocampus were measured using the DuoSet ELISA kits from R&D Systems following the manufacturer's instructions (mouse IL-1 β/IL-1F2, catalog #DY401-05; mouse TNF-α, catalog #DY410-05). Briefly, the detection antibody was incubated in a 96-well ELISA plate overnight at room temperature. Then, on the following day, 50 ng (100 μl) of the samples and standard curve (IL-1β: from 15.6–1000 pg/ml; TNF-α: 31.2–2000 pg/ml) were added to the wells and incubated for 2 h at room temperature; 100 μl of streptavidin-HRP complex was added to the wells followed by a 20 min incubation. A color reaction, caused by the addition of a substrate solution (100 μl) and terminated via stopping solution (50 μl), was quantified at 450 and 570 nm using a microplate reader. Cytokine concentration was calculated following the manufacturer's recommendations; 570 nm values were subtracted from the 450 nm values. The log10 of the standard curve values were plotted, and a line of best fit was generated. The amount of cytokines was extrapolated using standard curve and average of calculated triplicate. Cytokine concentration was then normalized to milligrams of total protein concentration in tissue.

Fluoro-Jade B (FjB) staining. To assess status epilepticus-induced neurodegeneration, FjB staining was performed as described previously (Engel et al., 2018). Briefly, 12 μm coronal sections at the medial level of the hippocampus (bregma AP = −1.94 mm) were cut on a cryostat. Tissue was fixed in 4% PFA, rehydrated in ethanol, and then transferred to a 0.006% potassium permanganate solution followed by incubation with 0.001% FjB (Millipore Bioscience Research Reagents). Sections were mounted in DPX mounting solution. Then, using an epifluorescence microscope, cells, including all hippocampal subfields (DG, CA1, and CA3), were counted under a 40× lens in two adjacent sections and the average determined for each animal.

Histopathology. For histopathological analysis, sections were fixed in 4% PFA and permeabilized with 3% Triton. Sections were then blocked in 5% goat serum and incubated overnight with the specific cell type marker GFAP (1/400) (RRID:AB_477035, 1/1000) (Sigma-Aldrich) or Iba1 (RRID:AB_839504, 1/400) (Wako). The following day, sections were washed in PBS and incubated with secondary antibodies conjugated to AlexaFluor-568 or -488 (BioSciences) for 2 h at room temperature. Then, sections were washed in PBS, stained with DAPI, washed again, and mounted using FluorSave (Merck Millipore). Two images from each hippocampal subfield were obtained using a 40× lens in the Nikon 2000s epifluorescence microscope. Cell counts were the result of the average counting of both images and were performed unaware of treatment groups.

Immunofluorescence confocal microscopy. Mice were transcardially perfused with 4% PFA and postfixed for an additional 24 h. Brains were then transferred to PBS and immersed into 4% agarose before sectioning; 30 μm sagittal sections were cut using the VT1000S vibratome (Leica Microsystems) and sections stored at −20°C in glycol. For immunofluorescence staining, tissue sections were incubated with 0.1% Triton/PBS and 1 M glycine, followed by blocking with 1% BSA in PBS for 45 min. Then, sections were incubated with the primary antibody anti-$P2Y_1$ (catalog #377324, 1:100, Santa Cruz Biotechnology) overnight. This was followed by washing with PBS and a second incubation for 2 h at room temperature with a second primary antibody against NeuN (RRID: AB_10807945, 1:400, Millipore), GFAP (RRID:AB_477035, 1:400, Sigma-Aldrich), S100β (RRID:AB_2620024, 1:400, Synaptic Systems), or Iba1 (RRID:AB_839504, 1:400, Wako). After washing in PBS, tissue was incubated with fluorescent secondary antibodies (AlexaFluor-488 or AlexaFluor-568 (BioSciences). This was again followed by washing in PBS and a short incubation with DAPI. FluorSave was used to cover the tissue, and confocal images were taken with a TCR 6500 microscope (Leica Microsystems) equipped with four laser lines (405, 488, 561, and

653 nm) using a 40× immersion oil objective (NA 1.3; Leica Microsystems).

Hippocampal primary neuron culture and cell death assays. Primary cultures of hippocampal neurons were prepared using E18 embryonic mice (C57BL/6) as described previously (Engel et al., 2017a). Hippocampal neurons were plated onto a poly-L-lysine and laminin bed and incubated in 10% horse serum in Neurobasal medium for 3 h at 37°C to allow the cells to adhere to the coverslip lining the bottom of the well in a M24 plate. After 3 h, neurobasal medium was removed completely and replaced by N2/B27/Neurobasal medium: N2 (Invitrogen), B27 (Invitrogen), 2 mM glutamine, 2 mM pyruvate, and 100 U/ml penicillin/streptomycin in Neurobasal medium. Cells were incubated at 37°C in a humidified atmosphere with 5% (v/v) CO_2 for 7–10 d (every 2 d, 50% of the N2/B27/Neurobasal medium was replaced by a fresh medium). Hippocampal neurons were transfected at 6 DIV with 1 μg of pCMV6-*GFP* or pCMV6-*P2ry1R-GFP* plasmid (catalog #MG226766; Origen) using the calcium-phosphate technique (Engel et al., 2017a). Twenty-four hours after transfection, hippocampal neurons were pretreated with Veh or 10 μM of $P2Y_1$ antagonist MRS25 for 30 min, which was followed by treatment with 0.3 μM KA for 5 h at 37°C. Neurons were then stained with Hoechst 33258 (1:1000); and to detect cell death, propidium iodide (1:1000) was added to the medium for 20 min. Nuclear morphology was assessed with an epifluorescence microscope using a 20× objective. For each condition, images of nuclei were captured from six different areas for each individual well. GFP- and propidium iodide-positive cells showing condensed and/or fragmented nuclei were scored as dead and expressed as a percentage of the total GFP-positive cell population. $N = 6$ indicates 6 independent pups from 3 litters. Every point represents the average of 3 independent wells (technical replicates).

Intracellular calcium measurements using Fluo4 AM. Primary hippocampal neurons on Willco dishes (Willco Wells) were coloaded with the calcium dye, Fluo-4 AM (3 μM) for 30 min at 37°C (in the dark) in experimental buffer containing 120 mM NaCl, 3.5 mM KCl, 0.4 mM KH_2PO_4, 20 mM HEPES, 5 mM $NaHCO_3$, 1.2 mM Na_2SO_4, 1.2 mM $CaCl_2$, and 15 mM glucose at pH 7.4. Cells were washed and bathed in 2 ml of experimental buffer containing TMRM, and a thin layer of mineral oil was added to prevent evaporation. Neurons were placed on the stage of an LSM 7.10 confocal microscope equipped with a 63 × 1.4 NA oil-immersion objective and a thermostatically regulated chamber set at 37°C (Carl Zeiss). Following a baseline equilibration time (30 min), MRS25 (10 μM) was dissolved in experimental buffer and was added to the medium. Fluo-4 was excited at 488 nm, and the emission was collected through a 505–550 nm barrier filter. Images were captured every 30 s during antagonist (MRS25) exposure. All images were processed and analyzed using MetaMorph Software version 7.5 (Universal Imaging). Data presented was normalized to the baseline.

Microglia cell culture. Microglia cells were obtained from C57BL/6 pups at postnatal day 5 (P5). P5 pups were decapitated, and skin and skull were removed carefully to avoid damage to the brain. The cerebellum was discarded, and the cortex and hippocampus were transferred to 10% FBS/DMEM: DMEM containing 10% FBS (v/v), 100 U/ml penicillin, and 100 mg/ml streptomycin. A total of 8 brains (16 hemispheres) were pooled together and cut into small pieces, followed by incubation in 5 ml of trypsin-EDTA in a water bath at 37°C for 15 min. Trypsin was then neutralized by adding 20 ml of DMEM, containing 10% FBS and tissue was centrifuged at 1500 rpm for 3 min. The supernatant media was removed, and 10 ml of fresh 10% FBS/DMEM was added. Using a 1 ml pipette, tissue was triturated until all tissue was dissociated. Cells were then counted using a hemocytometer. Cells were plated at 100,000 cells/cm^2 into different T75 flasks (75 cm^2). The flasks containing the cells were incubated at 37°C with 5% CO_2; and every 2–3 d, the medium was removed and replaced with fresh medium. After 12–14 d, astrocytes were confluent and overlaying microglia. Microglia isolation was performed by orbital shaking, placing the T75 flasks on a plate shaker at 250 rpm for 2 h. The media containing the floating microglia were centrifuged at 1500 rpm for 5 min and pellet resuspended in DMEM containing 10% FBS medium. Cells were counted and plated in a density of 10,000 cells/cm^2 in a 6-well plate. Microglia were treated with 100 μM/10 mM of glutamate/glycine or 100 μM/10 mM of glutamate/glycine and 10 μM MRS25 in 1% FBS/DMEM for 2 h. Next, cells were washed in PBS and fixed with 4% PFA. For immunocytofluorescence staining, coverslips were incubated with blocking solution (10% BSA, 5% FBS, and 2% Triton) for 1 h. Then, cells were incubated with the primary antibodies against $P2Y_1$ (1/100, Santa Cruz Biotechnology) and Iba1 (1/400, Wako), washed three times with PBS/BSA 3%, incubated with the secondary antibody (AlexaFluor-488 or AlexaFluor-568, BioSciences) for 1 h, and stained with DAPI. Cells were mounted using FluorSave, and 10 pictures (20×) per coverslip taken. Microglia-positive cells (Iba1) were counted in both treatments using ImageJ. Ratio of resting/reactive was established analyzing the activation stage of microglia in both treatments.

Experimental design and statistical analysis. All experiments were performed using male mice 8–12 weeks of age. Statistical design for experiments, including control groups, group size, and statistical test, can be found in Results. Statistical analysis of data was performed using Prism 5 (GraphPad) and STATVIEW software (SAS Institute). Data are mean ± SEM. One-way ANOVA parametric statistics with *post hoc* Fisher's protected least significant difference test was used to determine statistical differences between three or more groups. Unpaired Student's *t* test was used for two-group comparison. Two-way ANOVA was used for repeated measures between groups where a series of measurements have been taken from the same mouse at different time points. Survival was calculated using a log-rank test, with survival censored at 24 h after status epilepticus for animals remaining alive at this time point.

Results

Microglial and neuronal expression of $P2Y_1$ following status epilepticus

$P2Y_1$ receptor expression throughout different regions of the brain, including the hippocampus, is well established (Webb et al., 1998; Moore et al., 2000; Burnstock, 2007). Using chemoconvulsant-induced mouse models of status epilepticus, we have previously demonstrated an increase in $P2Y_1$ expression in the hippocampus following status epilepticus (Alves et al., 2017). The cell types involved remained, however, unexplored. To elucidate the cell-specific expression of $P2Y_1$ following status epilepticus, we used the well-characterized intra-amygdala KA mouse model of focal-onset status epilepticus (Fig. 1*A*) (Mouri et al., 2008). As reported previously, intra-amygdala KA-induced status epilepticus leads to neurodegeneration in different parts of the ipsilateral brain hemisphere, particularly in the inner layers of the cortex and the CA3 region of the hippocampus, whereas the contralateral side remains mainly spared from cell death. All mice treated with intra-amygdala KA will develop epilepsy following a short latency period of 3–5 d (Mouri et al., 2008).

To investigate the cell types in the hippocampus in which $P2Y_1$ expression is increased, we performed double immunofluorescence staining against the $P2Y_1$ receptor and different cell markers, including the neuronal marker NeuN, the microglia marker Iba1, and the astrocyte markers GFAP and S100β (Fig. 1*B*). Under control conditions, hippocampal $P2Y_1$ expression was restricted largely to NeuN-positive cells, suggesting a mainly neuronal expression under physiological conditions (Fig. 1*B*). At 8 h following status epilepticus, neuronal $P2Y_1$ expression increased, localized mainly to the cell soma, and was also detected on microglia. This pattern persisted up to at least 24 h following KA injection (Fig. 1*B*). Surprisingly, no colocalization was observed with the astrocyte markers GFAP or S100β, either under control conditions or at 8 or 24 h after status epilepticus (Fig. 1*B*). Specificity of the antibody was confirmed by the absence of immunoreactivity in tissue from *P2Y*$_1$ *KO* ($P2Y_1^{-/-}$) mice (Fig. 1*C*). $P2Y_1$ functioning on neurons was confirmed using

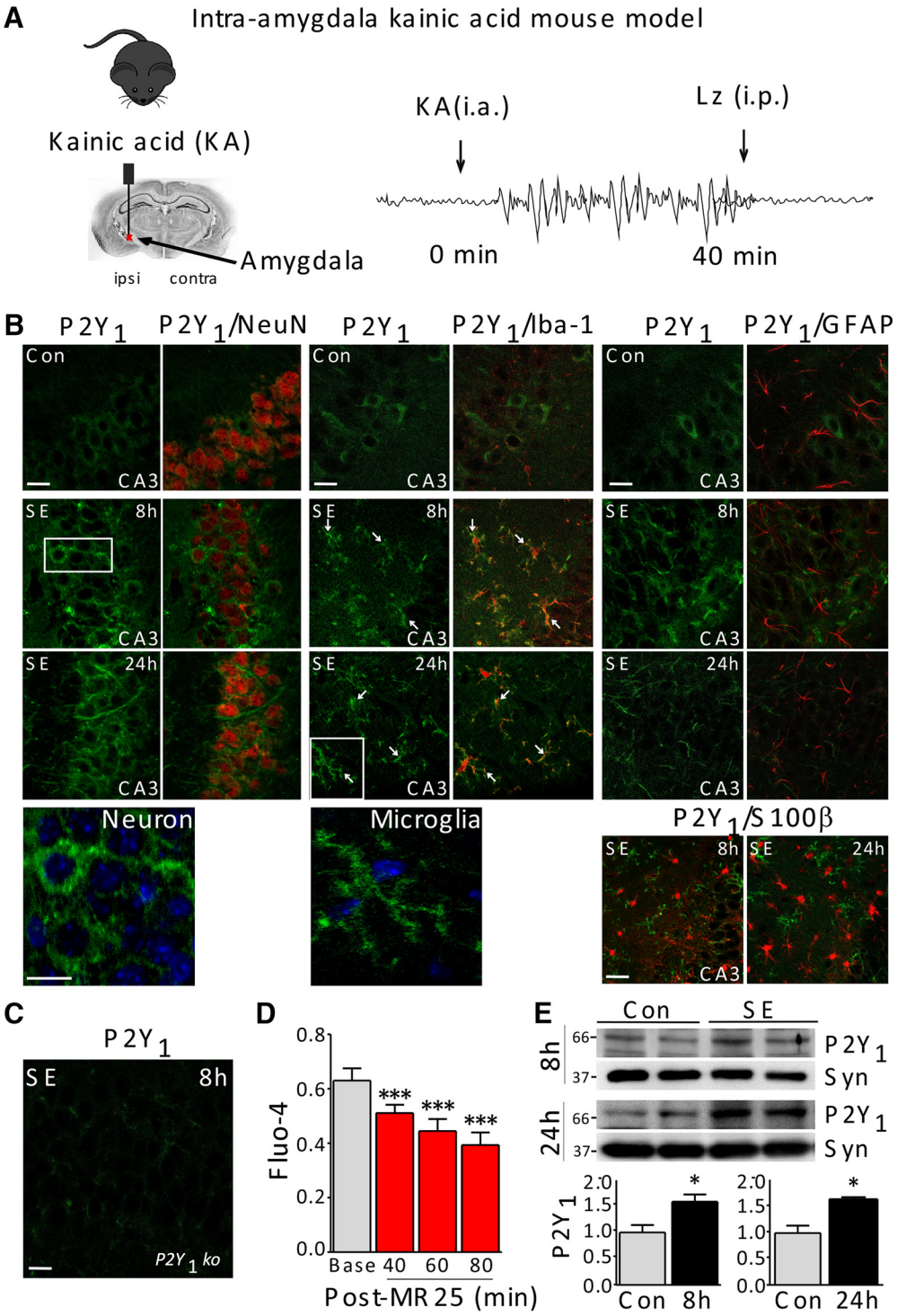

Figure 1. Increased neuronal and microglial $P2Y_1$ expression following status epilepticus. ***A***, Intra-amygdala KA-induced status epilepticus mouse model. Status epilepticus is triggered via an injection of 0.3 μg KA into the basolateral nucleus of the ipsilateral amygdala. First seizure bursts appear usually within minutes, gradually developing into status epilepticus. To reduce mortality and morbidity, the anticonvulsant lorazepam (Lz) is administered 40 min following KA injection. ***B***, Photomicrograph (40× lens) showing colocalization of $P2Y_1$ (green) with neurons and microglia 8 h and 24 h following status epilepticus (SE) in the CA3 region of the hippocampus. Scale bar, 10 μm. $P2Y_1$ (green) does not colocalize with the astrocyte markers GFAP and S100β (red). White arrows indicate colocalization of $P2Y_1$ with microglia. Bottom, Higher magnification of $P2Y_1$-positive neuron (8 h after status epilepticus) and $P2Y_1$-positive microglia (24 h after status epilepticus). ***C***, Specificity of $P2Y_1$-detecting antibody was confirmed using tissue from *$P2Y_1$ KO* mice (ko) 8 h after status epilepticus. Scale bar, 50 μm. ***D***, Graph showing decreased intracellular Ca^{2+} in neurons following treatment with the $P2Y_1$ antagonist MRS25 (10 μM) ($n = 3$ per group; one-way ANOVA with Fisher's *post hoc* test; Baseline [Base] vs 40 min: 0.6305 ± 0.04462 vs 0.5113 ± 0.0307, $F = 5.979$, df = 3, $p < 0.0001$; Base vs 60 min: 0.6305 ± 0.04462 vs 0.4453 ± 0.04385, $F = 5.979$, df = 3, $p < 0.0001$; Base vs 80 min: 0.06305 ± 0.04462 vs 0.3935 ± 0.04635, $F = 5.979$, df = 3, $p < 0.0001$). ***E***, Western blot (each lane = 2 hippocampi) and respective graphs showing a significant increase of $P2Y_1$ in synaptoneurosomes at 8 h ($n = 4$ per group, unpaired Student's *t* test: 1.000 ± 0.1412 vs 1.588 ± 0.1378, $t = 2.979$, df = 6, $p = 0.025$) and 24 h after status epilepticus ($n = 3$ per group; unpaired Student's *t* test: 1.000 ± 0.2042 vs 1.630 ± 0.0378, $t = 3.034$, df = 4, $p = 0.039$). Synaptophysin (Syn) is shown as guide to loading. Data are mean ± SEM. *$p < 0.05$, ***$p < 0.001$.

primary hippocampal cell cultures, demonstrating decreased intracellular calcium levels after $P2Y_1$ inhibition (Fig. 1*D*). In addition, analysis of synaptoneurosomes taken at different time points from mice following status epilepticus revealed that $P2Y_1$ expression is significantly increased at hippocampal synapses at both 8 and 24 h after status epilepticus (Fig. 1*E*).

These data demonstrate that, in the hippocampus, $P2Y_1$ is expressed on neurons under physiological conditions and is upregulated following status epilepticus, particularly in microglia and at postsynaptic sites on neurons.

Genetic ablation of $P2Y_1$ exacerbates seizure severity and resulting neuronal death

To obtain genetic evidence that $P2Y_1$ signaling can affect seizures or seizure-induced pathology, we explored the outcome of status epilepticus in $P2Y_1^{-/-}$ and $P2Y_1$ heterozygous ($P2Y_1^{+/-}$, het) mice. First, we investigated whether loss of $P2Y_1$ altered basal expression of key glial cell markers and neurotransmitter receptors. Western blot analysis of protein extracts from the hippocampus of naive $P2Y_1^{-/-}$ mice revealed significantly lower concentrations of GFAP and Iba1 in the hippocampus compared with WT mice (Fig. 2*A*,*B*). While no difference was observed in the expression of $GABA_A$, $P2Y_2$, $P2Y_{12}$, and $P2Y_{13}$ receptors between WT and $P2Y_1^{-/-}$ mice, expression of the kainate receptor GluR6/7 was higher in $P2Y_1^{-/-}$ mice (Fig. 2*A*,*B*).

We then investigated the impact of $P2Y_1$ deficiency on status epilepticus. No difference was found in baseline EEG recordings between WT and $P2Y_1^{-/-}$ mice (total power: 30,790 ± 2634 μV^2 WT vs 27,630 ± 6267 μV^2 $P2Y_1^{-/-}$, $p = 0.70$, unpaired Student's t test). Following KA injection, however, $P2Y_1^{-/-}$ and $P2Y_1^{+/-}$ mice showed a decreased latency to the first seizure, compared with WT (Fig. 2*C*,*D*). Both $P2Y_1^{-/-}$ and $P2Y_1^{+/-}$ mice also displayed significantly higher total power and amplitude on the EEG during status epilepticus and during a 60 min recording period following lorazepam administration compared with WT mice (Fig. 2*C*,*E*,*F*).

We next investigated the effect of $P2Y_1$ deficiency on the neuroanatomical consequences of status epilepticus. As expected, both $P2Y_1^{-/-}$ and $P2Y_1^{+/-}$ mice displayed increased neuronal death following status epilepticus, as evidenced by more FjB-positive cells in the hippocampus, compared with WT mice. This difference was mainly found in the cell death-prone CA3 subfield (Fig. 2*G*,*H*). In contrast to cell death, tissue sections from $P2Y_1^{-/-}$ and $P2Y_1^{+/-}$ mice displayed fewer astrocytes in the hippocampus compared with WT mice (Fig. 2*I*,*J*).

In summary, $P2Y_1$ deficiency predisposes the brain to experience more severe seizures during status epilepticus with a resulting increase in neurodegeneration.

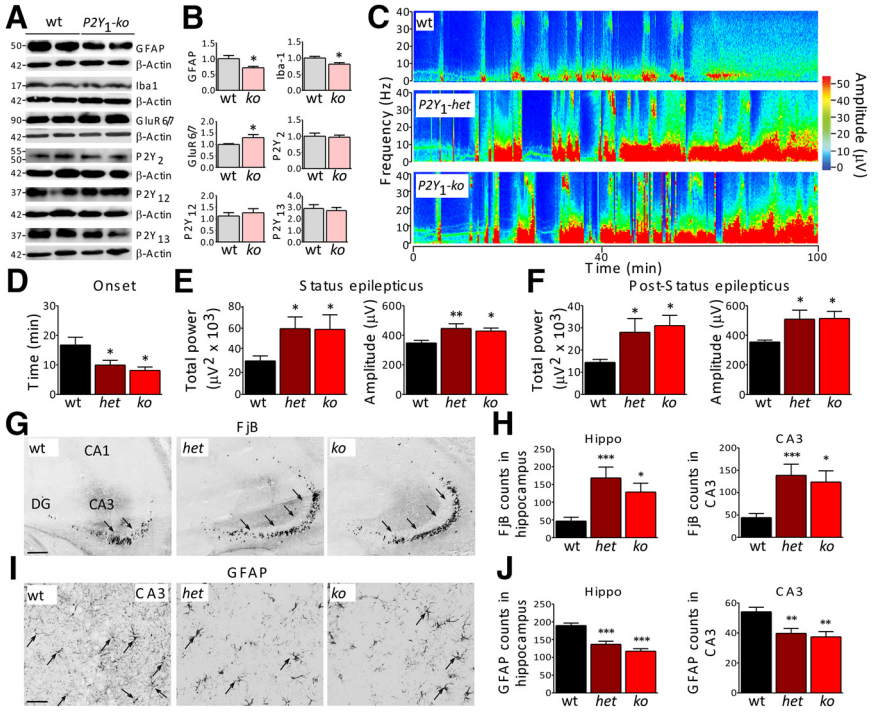

Figure 2. $P2Y_1$ deficiency increases seizure severity and neuronal death in the intra-amygdala KA mouse model. ***A***, Western blot ($n = 1$ per lane) using hippocampal tissue from naive WT and $P2Y_1^{-/-}$ *mice* (*ko*). ***B***, Corresponding graphs showing decreased protein levels of GFAP and Iba1 (GFAP: wt vs *ko*: 1.000 ± 0.1021 vs 0.7141 ± 0.0454, $t = 2.559$, df = 10, $p = 0.028$; Iba1: wt vs *ko*: 1.000 ± 0.051 vs 0.8112 ± 0.0436, $t = 2.813$, df = 10, $p = 0.018$). GluR6/7 protein levels are increased in $P2Y_1^{-/-}$ (*ko*) mice (wt vs *ko*: 1.000 ± 0.0348 vs 1.299 ± 0.1300, $t = 2.421$, df = 9, $p = 0.039$). No differences in protein levels of $P2Y_2$, $P2Y_{12}$, and $P2Y_{13}$ were observed between genotypes. β-Actin is shown as guide to loading ($n = 6$ per group, unpaired Student's t test). ***C***, Representative EEG recordings presented as heat maps of frequency and amplitude data during status epilepticus of WT, $P2Y^{+/-}$ (*het*), and $P2Y^{-/-}$ (*ko*) mice. ***D***, Graph showing a faster onset of seizures in $P2Y^{+/-}$ (*het*) and $P2Y^{-/-}$ (*ko*) mice compared with WT mice ($n = 14$ (WT), $n = 13$ ($P2Y^{+/-}$), and $n = 11$ ($P2Y^{-/-}$) (one-way ANOVA with Fisher's *post hoc* test; wt vs $P2Y^{+/-}$: 8.322 ± 1.229 min vs 4.947 ± 0.728 min, $F = 3.698$, df = 2, $p = 0.030$ and wt vs $P2Y^{-/-}$: 8.322 ± 1.229 min vs 4.554 ± 0.726 min, $F = 3.698$, df = 2, $p = 0.032$). ***E***, Graphs showing increased EEG total power and amplitude during a 40 min recording period starting from the injection of KA until lorazepam administration (status epilepticus) ($n = 14$ (WT), $n = 13$ ($P2Y^{+/-}$), and $n = 11$ ($P2Y^{-/-}$) (one-way ANOVA with Fisher's *post hoc* test; total power: wt vs $P2Y^{+/-}$: 30,360 ± 4574 μV^2 vs 59,520 ± 10,550 μV^2, $F = 3.203$, df = 2, $p = 0.032$ and wt vs $P2Y^{-/-}$: 30,360 ± 4574 μV^2 vs 58,880 ± 13,170 μV^2, $F = 3.203$, df = 2, $p = 0.044$; amplitude: wt vs $P2Y^{+/-}$: 348.0 ± 17.77 μV vs 446.0 ± 31.10 μV, $F = 4.849$, df = 2, $p = 0.006$ and wt vs $P2Y^{-/-}$: 348.0 ± 17.77 μV vs 428.2 ± 19.96 μV, $F = 4.849$, df = 2, $p = 0.033$) and (***F***) during a 60 min recording period following lorazepam (after status epilepticus) in $P2Y^{+/-}$ (*het*) and $P2Y^{-/-}$ (*ko*) mice compared with WT mice ($n = 14$ (WT), $n = 13$ ($P2Y^{+/-}$), and $n = 11$ ($P2Y^{-/-}$) (one-way ANOVA with Fisher's *post hoc* test; total power: wt vs $P2Y^{+/-}$: 14,440 ± 1374 μV^2 vs 27,970 ± 6170 μV^2, $F = 4.031$, df = 2, $p = 0.029$ and wt vs $P2Y^{-/-}$: 14,440 ± 1374 μV^2 vs 30,980 ± 4643 μV^2, $F = 4.031$, df = 2, $p = 0.018$; amplitude: wt vs $P2Y^{+/-}$: 354.8 ± 12.74 μV vs 508.6 ± 60.50 μV, $F = 4.507$, df = 2, $p = 0.014$ and wt vs $P2Y^{-/-}$: 354.8 ± 12.74 μV vs 513.7 ± 47.73 μV, $F = 4.507$, df = 2, $p = 0.018$). ***G***, Photomicrographs (10× lens) and (***H***) graphs showing more FjB-positive cells in the ipsilateral hippocampus and CA3 subfield of the hippocampus 24 h after status epilepticus in $P2Y^{+/-}$ (*het*) and $P2Y^{-/-}$ (*ko*) mice compared with WT mice ($n = 14$ (WT), $n = 13$ ($P2Y^{+/-}$), and $n = 11$ ($P2Y^{-/-}$) (one-way ANOVA with Fisher's *post hoc* test; whole hippocampus: wt vs $P2Y^{+/-}$: 46.73 ± 10.84 vs 168.4 ± 30.37, $F = 9.273$, df = 2, $p = 0.0002$ and wt vs $P2Y^{-/-}$, 46.73 ± 10.84 vs 128.6 ± 24.77, $F = 9.273$, df = 2, $p = 0.023$; CA3: wt vs $P2Y^{+/-}$: 44.20 ± 9.134 vs 138.7 ± 24.87, $F = 8.306$, df = 2, $p = 0.0006$ and wt vs $P2Y^{-/-}$: 44.20 ± 9.134 vs 123.7 ± 25.10, $F = 8.306$, df = 2, $p = 0.010$). Scale bar, 200 μm. ***I***, Representative GFAP staining (40× lens) and (***J***) graphs showing a decrease in the number of astrocytes in the ipsilateral hippocampus and CA3 subfield of the hippocampus 24 h following status epilepticus in $P2Y^{+/-}$ (*het*) and $P2Y^{-/-}$ (*ko*) mice compared with WT mice ($n = 14$ (WT), $n = 13$ ($P2Y^{+/-}$), and $n = 11$ ($P2Y^{-/-}$) (one-way ANOVA with Fisher's *post hoc* test; whole hippocampus: wt vs $P2Y^{+/-}$: 189.7 ± 7.065 vs 137.1 ± 8.532, $F = 22.20$, df = 2, $p = 0.0001$ and wt vs $P2Y^{-/-}$: 189.7 ± 7.065 vs 117.6, $F = 22.20$, df = 2, $p = 0.0001$; CA3: wt vs $P2Y^{+/-}$: 54.11 ± 3.010 vs 39.75 ± 3.256, $F = 7.748$, df = 2, $p = 0.0022$ and wt vs $P2Y^{-/-}$: 54.11 ± 3.010 vs 37.42 ± 3.515, $F = 7.748$, df = 2, $p = 0.0039$). Scale bar, 50 μm. Data are mean ± SEM. $^*p < 0.05$, $^{**}p < 0.01$, $^{***}p < 0.001$.

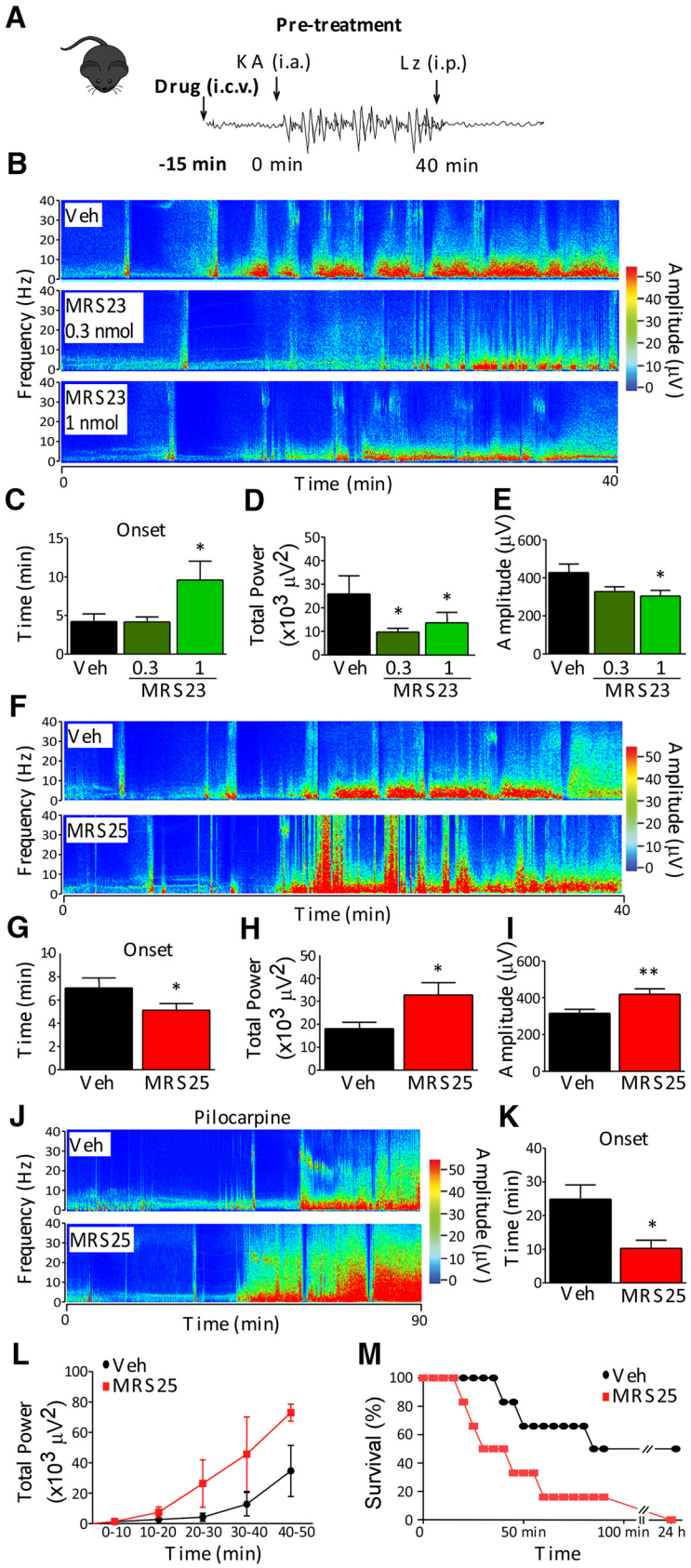

Figure 3. Activation of the $P2Y_1$ receptor decreases seizure severity during status epilepticus. ***A***, Experimental design of pre-treatment regimen. Mice were treated with the $P2Y_1$ agonist MRS23 or antagonist MRS25 15 min before intra-amygdala KA injection. Lorazepam (Lz) was administered 40 min following KA injection. ***B***, Heat maps of frequency and amplitude data during status epilepticus in mice treated with the $P2Y_1$ agonist MRS23 (0.3 or 1 nmol) or Veh. ***C***, Significant delay in the time to fist seizure burst (seizure onset) in mice pretreated with $P2Y_1$ agonist MRS23 (1 nmol) ($n = 14$ Veh), $n = 9$ (0.3 nmol MRS23), and $n = 11$ (1 nmol MRS23) (one-way ANOVA with Fisher's *post hoc* test; Veh vs 1 nmol: 4.222 ± 0.9901 min vs 9.612 ± 2.426 min, $F = 3.824$, df = 2, $p = 0.020$). ***D***, ***E***, Reduced EEG total power and amplitude during a 40 min recording period starting from KA injection until lorazepam administration (status epilepticus) in mice treated with the $P2Y_1$ agonist MRS23 ($n = 14$ Veh, $n = 9$ (0.3 nmol MRS23), and $n = 11$ (1 nmol MRS23) (one-way ANOVA with Fisher's *post hoc* test; total power: Veh vs 0.3 nmol: 35,880 ± 8388 μV^2 vs 15,150 ± 2740 μV^2, $F = 3.474$, df = 2, $p = 0.035$, Veh vs 1 nmol: 35,880 ± 8388 μV^2 vs 16,180 ± 3831 μV^2, $F = 3.474$, df = 2, $p = 0.034$; amplitude: Veh vs 0.3 nmol: 427.6 ± 44.77 μV vs 327.5 ± 25.55 μV, $F = 3.297$, df = 2, $p = 0.077$, Veh vs 1 nmol: 427.6 ± 44.77 μV vs 304.1 ± 29.39 μV, $F = 3.297$, df = 2, $p = 0.023$). ***F***, Representative EEG recordings presented as heat maps of frequency and amplitude data during status epilepticus in mice treated with the $P2Y_1$ antagonist MRS25 or Veh. ***G***, Earlier seizure onset in $P2Y_1$ agonist MRS25-treated mice ($n = 13$ per group; unpaired Student's *t* test: 7.045 ± 0.863 min vs 5.126 ± 0.5744 min, $t = 1.850$, df = 28, $p = 0.043$). ***H***, ***I***, Increased EEG total power and amplitude during status epilepticus in $P2Y_1$ antagonist MRS25-treated mice compared with Veh-treated mice ($n = 13$ per group; unpaired Student's *t* test; total power: 18,110 ± 2764 μV^2 vs 32,770 ± 5390 μV^2, $t = 2.420$, df = 24, $p = 0.023$; amplitude: 315.4 ± 20.59 μV vs 418.5 ± 28.95 μV, $t = 2.902$, df = 24, $p = 0.0078$). ***J***, Representative EEG recordings represented as heat maps of frequency and amplitude data in pilocarpine-injected mice treated with $P2Y_1$ antagonist MRS25 or Veh. ***K***, Earlier seizure onset in mice treated with the $P2Y_1$ antagonist MRS25 ($n = 6$ per group; unpaired Student's *t* test: 24.88 ± 4.237 min vs 10.27 ± 2408 min, $t = 2.859$, df = 11, $p = 0.016$). ***L***, Graph showing EEG total power in mice treated with $P2Y_1$ antagonist MRS25 and Veh in the pilocarpine mouse model ($n = 6$ per group). ***M***, Graph showing decreased survival in MRS25-treated mice compared with Veh-injected mice following pilocarpine injection ($n = 10$ per group; $\chi^2 = 133.0$, df = 181). Data are mean ± SEM. *$p < 0.05$, **$p < 0.01$.

$P2Y_1$ activation before the induction of status epilepticus reduces seizure severity

To complement and extend our genetic studies, we used a pharmacological approach, taking advantage of the availability of the specific $P2Y_1$ antagonist MRS2500 (MRS25) and agonist MRS2365 (MRS23) (von Kügelgen and Hoffmann, 2016). Status epilepticus was induced as before, and MRS25 or MRS23 were delivered into the lateral ventricle 15 min before intra-amygdala KA injection (Fig. 3*A*).

In line with the increased seizure severity observed in $P2Y_1^{-/-}$ mice, injection with the $P2Y_1$ agonist MRS23 before status epilepticus delayed seizure onset and reduced EEG total power and amplitude during status epilepticus (Fig. 3*B–E*). EEG continued to show a trend to lower total power in MRS23-treated mice for at least 60 min following lorazepam administration (total power: 25,910 ± 7674 μV^2 Veh vs 9724 ± 1588 μV^2, 0.3 nmol, $p = 0.07$;

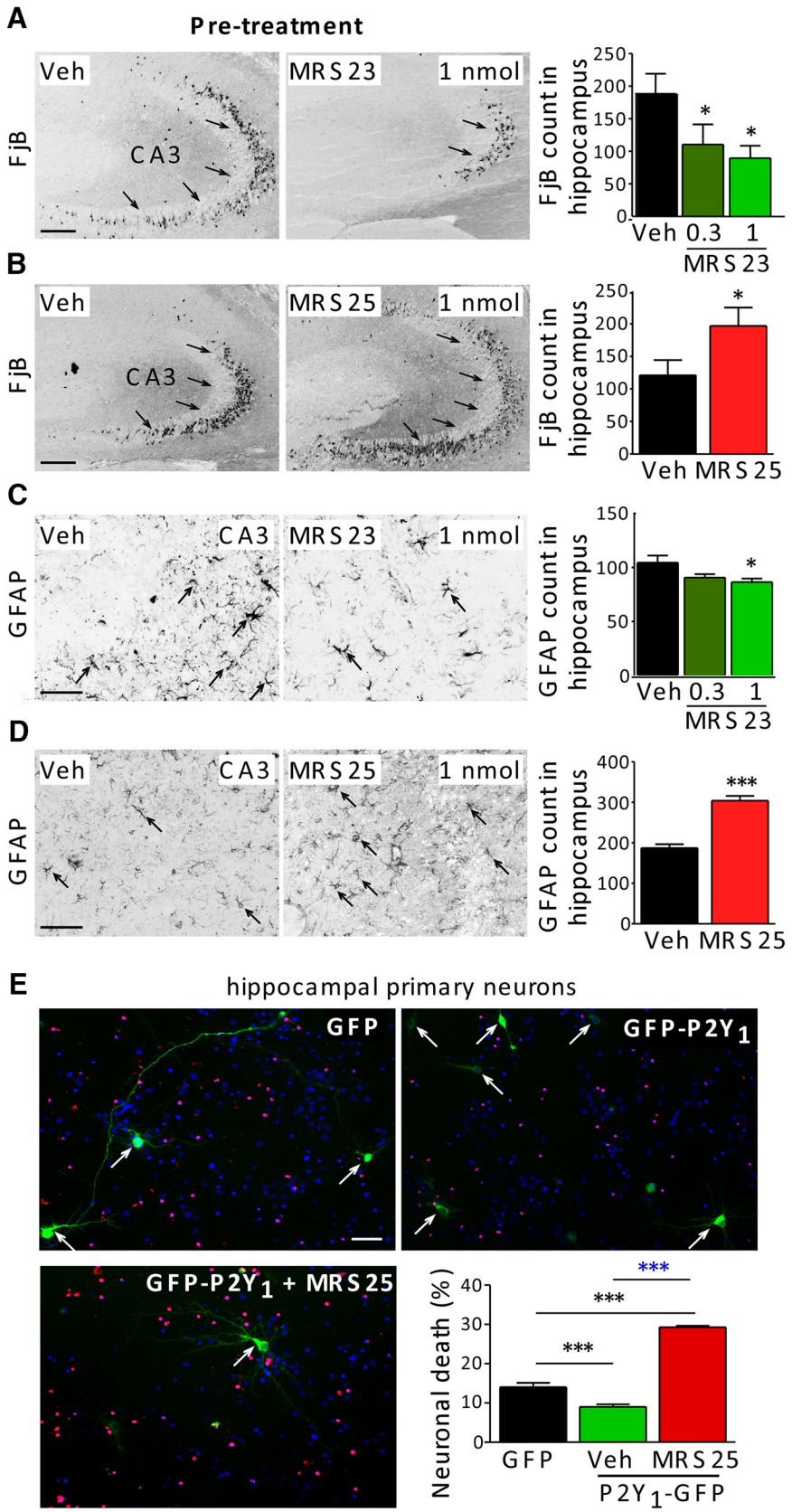

Figure 4. Activation of the $P2Y_1$ receptor reduces cell death and astrogliosis after status epilepticus. ***A***, Photomicrographs (10× lens) and graph showing significant less FjB-positive cells in the hippocampus 24 h after status epilepticus in mice treated with $P2Y_1$ agonist MRS23 (0.3 and 1 nmol) ($n = 14$ Veh), $n = 9$ (0.3 nmol MRS23), and $n = 11$ (1 nmol MRS23; one-way ANOVA with Fisher's *post hoc* test; Veh vs 0.3 nmol: 188.5 ± 30.68 vs 110.5 ± 30.82, $F = 3.873$, df = 2, $p = 0.043$; Veh vs 1 nmol: 188.5 ± 30.68 vs 89.46 ± 18.89, $F = 3.873$, df = 2, $p = 0.012$). Scale bar, 200 μm. ***B***, Representative photomicrograph (10× lens) and corresponding graph showing more FjB-positive cells in the hippocampus 24 h after status epilepticus in mice treated with the $P2Y_1$ antagonist MRS25 ($n = 13$ per group; unpaired Student's *t* test: 121.2 ± 23.20 vs 197.0 ± 28.18, $t = 2.048$, df = 17, $p = 0.044$). Scale bar, 200 μm. ***C***, Representative GFAP staining (40× lens) and corresponding graph showing fewer astrocytes in the hippocampus in mice pretreated with the $P2Y_1$ agonist MRS23 ($n = 14$ Veh, $n = 9$, 0.3 nmol MRS23, and $n = 11$, 1 nmol MRS23; one-way ANOVA with Fisher's *post hoc* test; Veh vs 0.3 nmol: 104.6 ± 6.423 vs 90.70 ± 3.118, $F = 4.511$, df = 2, $p = 0.083$; Veh vs 1 nmol: 104.6 ± 6.423 vs 86.61 ± 3.088, $F = 4.511$, df = 2, $p = 0.044$). Arrows indicate GFAP-positive cells. Scale bar, 50 μm. ***D***, Representative GFAP images of hippocampus (40× lens) and correspondent graph showing more astrocytes in the hippocampus in mice pretreated with the $P2Y_1$ antagonist MRS25 ($n = 13$ per group; unpaired Student's *t* test: 187.1 ± 9.293 vs 304.0 ± 11.93, $t = 7.467$, df = 18, $p < 0.0001$). Arrows indicate GFAP-positive cells. Scale bar, 50 μm. ***E***, Representative image (20× lens) and corresponding graph revealing a significant reduction in the percentage of neuronal cell death in hippocampal neurons transfected with a GFP-$P2Y_1$ plasmid after KA treatment compared with the GFP-expressing control group. This protection was reversed in the presence of the $P2Y_1$ antagonist MRS25 ($n = 6$ per group; one-way ANOVA with Fisher's *post hoc* test; GFP vs Veh-$P2Y_1$-GFP: 14.05 ± 1.067 vs 9.021 ± 0.6350, $F = 199.4$, df = 2, $p = 0.0002$; GFP vs MRS25-$P2Y_1$-GFP: 14.05 ± 1.067 vs 29.29 ± 0.3664, $F = 199.4$, df = 2, $p < 0.0001$, Veh-$P2Y_1$-GFP vs MRS25-$P2Y_1$-GFP: 9.021 ± 0.6350 vs 29.29 ± 0.3664, $F = 199.4$, df = 2, $p < 0.0001$). Arrows indicate hippocampal neurons transfected with GFP and GFP-$P2Y_1$. Scale bar, 40 μm. Data are mean ± SEM. *$p < 0.05$, ***$p < 0.001$.

25,910 ± 7674 μV^2 Veh vs 13,630 ± 4436 μV^2, 1 nmol, $p = 0.15$; one-way ANOVA with Fisher's *post hoc* test). Conversely, and consistent with genetic findings on *$P2Y_1$* deficiency resulting in a more severe seizure phenotype, mice pretreated with the $P2Y_1$ antagonist MRS25 (1 nmol) displayed an earlier seizure onset and experienced increased seizure severity during status epilepticus (Fig. 3*F–I*). This increase, however not significant, was apparent up to 60 min after lorazepam injection (total power: 14,470 ± 2823 μV^2 Veh vs 26,520 ± 6782 μV^2 MRS25, $p = 0.11$; unpaired Student's *t* test).

To validate that our results were model-independent, we used another widely used mouse model of status epilepticus where seizures are induced with a systemic injection of the cholinergic agonist pilocarpine (Curia et al., 2008). Here, we used the $P2Y_1$ antagonist MRS25 (1 nmol), and, as before, mice were treated before the induction of status epilepticus. EEG was recorded for a period of 90 min during status epilepticus (Fig. 3*J*). As observed in the KA model, mice pretreated with the $P2Y_1$ antagonist MRS25 developed earlier seizure onset compared with Veh-treated mice (Fig. 3*J*,*K*). MRS25-treated mice also showed a trend to increased total power during status epi-

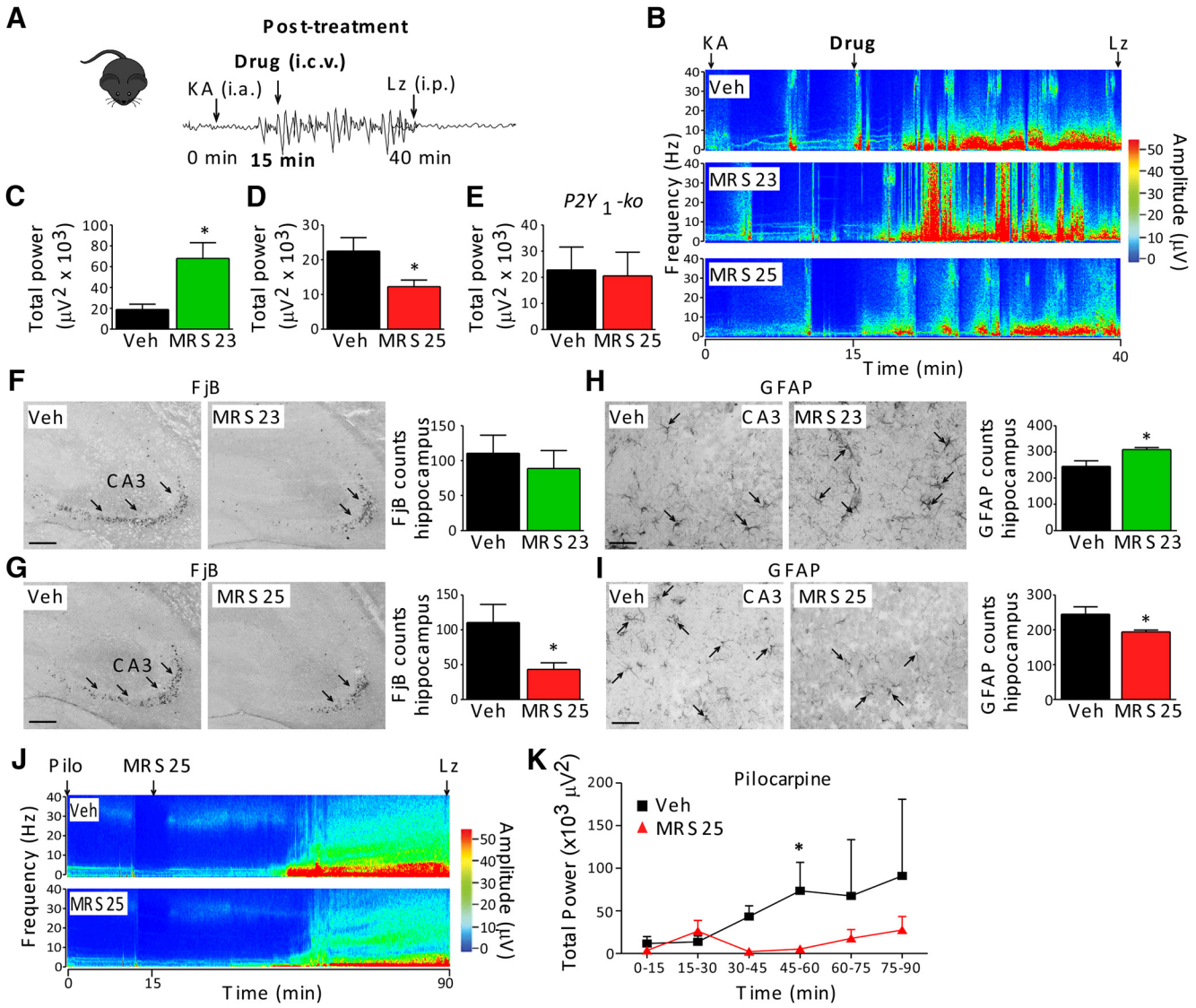

Figure 5. Pharmacological targeting of $P2Y_1$ during status epilepticus. ***A***, Experimental design of post-treatment regimen. At 15 min following intra-amygdala KA injection, mice were treated with the $P2Y_1$ agonist MRS23 or antagonist MRS25. Lorazepam (Lz) was administered 40 min following KA injection. ***B***, Representative EEG recordings presented as heat maps of frequency and amplitude data during status epilepticus in mice treated with Veh, MRS23, or MRS25. ***C***, Increased seizure severity in mice treated with the $P2Y_1$ agonist MRS23 ($n = 7$ Veh and $n = 9$ MRS23; unpaired Student's t test: $189.0 \pm 50.57\ \mu V^2$ vs $679.6 \pm 151.0\ \mu V^2$, $t = 2.753$, df $= 14$, $p = 0.016$). ***D***, Decreased seizure severity in mice treated with the $P2Y_1$ antagonist MRS25 compared with Veh-injected mice ($n = 7$ Veh and $n = 8$ MRS25; unpaired Student's t test: $224.9 \pm 39.014\ \mu V^2$ vs $122.7 \pm 19.04\ \mu V^2$, $t = 2.447$, df $= 13$, $p = 0.029$). Seizure total power was measured for both ***C*** and ***D*** from intracerebroventricular drug delivery (15 min after KA injection) until lorazepam administration, totaling 25 min. ***E***, Graph showing similar seizure total power during status epilepticus in $P2Y_1^{-/-}$ mice treated with the $P2Y_1$ receptor antagonist MRS25 or Veh, confirming specificity of MRS25 for $P2Y_1$ ($n = 4$ per group). MRS25 or Veh was administered 15 min following KA injection. ***F***, Representative images (10× lens) and graph showing no difference in FjB-positive cells 24 h after status epilepticus in mice treated with the $P2Y_1$ agonist MRS23 in the hippocampus ($n = 7$ Veh and $n = 9$ MRS23). Scale bar, 200 μm. ***G***, Representative images (10× lens) and corresponding graph showing less FjB-positive cells 24 h after status epilepticus in mice post-treated with the $P2Y_1$ receptor antagonist MRS25 ($n = 7$ Veh and $n = 8$ MRS25; unpaired Student's t test: 110.5 ± 26.04 vs 43.30 ± 9.439, $t = 2.642$, df $= 16$, $p = 0.018$). Scale bar, 200 μm. ***H***, Photomicrographs (40× lens) and graph showing an increase in GFAP-positive cells in the hippocampus 24 h after status epilepticus in mice treated with the $P2Y_1$ receptor agonist MRS23 ($n = 7$ Veh and $n = 9$ MRS23; unpaired Student's t test: 244.8 ± 21.35 vs 309.2 ± 7.826, $t = 2.292$, df $= 11$, $p = 0.043$). Scale bar, 50 μm. ***I***, Photomicrographs (40× lens) and corresponding graph showing fewer astrocytes in the hippocampus of mice treated with the $P2Y_1$ antagonist MRS25 ($n = 7$ Veh and $n = 8$ MRS25; unpaired Student's t test: 244.8 ± 21.35 vs 194.1 ± 5.221, $t = 2.553$, df $= 16$, $p = 0.021$). Scale bar, 50 μm. ***J***, Representative EEG recordings presented as heat maps of frequency and amplitude data during pilocarpine-induced status epilepticus in mice treated with the $P2Y_1$ antagonist MRS25 or Veh. ***K***, Decreased seizure severity in mice treated with the $P2Y_1$ receptor antagonist MRS25 compared with Veh-treated mice ($n = 10$ Veh and $n = 8$ MRS25; two-way ANOVA; Veh vs MRS25, 45–60 min: $F = 2.26$, $p < 0.05$). Data are mean ± SEM. *$p < 0.05$.

lepticus (Fig. 3*L*). Although in both treatment groups the percentage of mice entering status epilepticus was the same (60%), mortality during status epilepticus was different, with 50% of pilocarpine-treated mice surviving in the Veh group compared with 0% following treatment with MRS25, 24 h following pilocarpine injection (Fig. 3*M*).

In conclusion, $P2Y_1$, when activated before the induction of status epilepticus, reduces seizure onset and seizure severity.

$P2Y_1$ activation before the induction of status epilepticus protects against seizure-induced neuronal death

We next evaluated whether pretreatment with either the $P2Y_1$ agonist or antagonist affects seizure-induced cell death. Intra-amygdala KA-injected mice pretreated with the $P2Y_1$ agonist MRS23 displayed significantly fewer FjB-positive cells in the hippocampus (Fig. 4*A*), whereas mice pretreated with the $P2Y_1$ antagonist MRS25 showed a significant increase in FjB-positive cells

(Fig. 4*B*). Further, agonist MRS23-pretreated mice displayed decreased staining for the astrocyte marker GFAP compared with Veh mice after status epilepticus (Fig. 4*C*). In contrast, astrocyte staining was increased in the hippocampus of mice treated with the $P2Y_1$ antagonist MRS25 before status epilepticus (Fig. 4*D*).

To support the evidence that $P2Y_1$ activation protects against seizure-induced cell death, we treated primary hippocampal neurons transfected with GFP-$P2Y_1$ with KA. Cells expressing the receptor were identified by GFP-$P2Y_1$ fluorescence. KA treatment resulted in death of a significant percentage of primary hippocampal neurons. Neuronal death was significantly lower in GFP-$P2Y_1$-transfected hippocampal neurons treated with KA (Fig. 4*E*). GFP-$P2Y_1$ hippocampal neurons treated with the $P2Y_1$ receptor antagonist MRS25 30 min before KA treatment resulted in an increase in neuronal death, confirming that this effect was specific to the $P2Y_1$ receptor (Fig. 4*E*).

Together, our pharmacological approach confirms that $P2Y_1$, when activated before the induction of seizures, protects the brain from damage.

Treatment with $P2Y_1$ antagonist during status epilepticus reduces seizure severity and brain damage

Operationally, clinicians will initiate aggressive anti-seizure therapy if seizures continue beyond 5 min (Betjemann and Lowenstein, 2015). The above studies reveal that $P2Y_1$ receptor ligands may have therapeutic potential for status epilepticus. The pretreatment regimen, however, is not a clinically realistic scenario. Accordingly, we next performed experiments to test whether manipulating $P2Y_1$ after status epilepticus begins can alter seizure or pathologic outcomes. Mice received intracerebroventricular injections of either the $P2Y_1$ agonist MRS23 or antagonist MRS25 (both 1 nmol) 15 min following intra-amygdala KA injection, once mice had experienced at least one seizure burst (Fig. 5*A*).

Surprisingly, and in contrast to our pretreatment studies, injection of mice with the $P2Y_1$ agonist MRS23 shortly after KA injection resulted in an exacerbation of seizure severity during status epilepticus (Fig. 5*B*,*C*). Further demonstrating the opposing effects observed between pretreatment and post-treatment, seizure severity was reduced in mice injected with the $P2Y_1$ antagonist MRS25 15 min after KA injection (Fig. 5*B*,*D*). Confirming specificity of the $P2Y_1$ antagonist MRS25, no effect of MRS25 on seizure severity was observed during status epilepticus in *P2Y*$_1$-deficient mice (Fig. 5*E*).

To test whether brain pathology also differs between treatment regimens, we examined brain sections from mice from the post-treatment studies. FjB-positive hippocampal cell counts of $P2Y_1$ agonist MRS23-treated mice were similar to Veh-treated mice following status epilepticus (Fig. 5*F*). In contrast, antagonist-treated mice had lower counts of FjB-positive cells in the hippocampus compared with Veh-injected mice (Fig. 5*G*). Astrogliosis was significantly increased in the hippocampus of mice treated with the $P2Y_1$ agonist MRS23 (Fig. 5*H*) and reduced in the hippocampus of mice treated with the $P2Y_1$ antagonist MRS25 (Fig. 5*I*).

As before, to ensure the above findings were not unique to the intra-amygdala KA model, experiments were repeated in the pilocarpine model. Consistent with findings in the KA model, injection of mice with the $P2Y_1$ antagonist MRS25 15 min after pilocarpine injection reduced EEG total power (Fig. 5*J*,*K*). Further, in line with $P2Y_1$ antagonism being protective when administered following pilocarpine injection, fewer mice entered pilocarpine-induced status epilepticus (Veh 63% vs MRS25 53%) and the survival rate in MRS25-treated mice during status epilepticus was, in contrast to our pretreatment regimen, even slightly higher (47%) compared with Veh-injected mice (31%).

Together, in contrast to a pretreatment regimen, $P2Y_1$ seems to drive seizure pathology once status epilepticus has been triggered, with $P2Y_1$ antagonism being anticonvulsant.

$P2Y_1$-driven microglia activation contributes to seizures during status epilepticus

We next aimed to understand the mechanism via which modulating $P2Y_1$ activity can produce such a divergent response depending on when the receptor is targeted. One potential explanation is that, as seizures begin, there is a change in the cellular distribution of the receptor, potentially leading to different signaling pathways and responses than would occur under physiological conditions. As already described, we found a status epilepticus-induced increase in microglial $P2Y_1$ expression (Fig. 1*B*). Microglia are one of the first cell types to respond to injury, mediated via extracellular ATP (Davalos et al., 2005). We therefore hypothesized that microglia may be activated by the $P2Y_1$ receptor in a manner similar to that reported for other P2 receptors, such as P2X7 (Beamer et al., 2017).

To test this hypothesis, we first performed immunostaining on brain tissue sections collected 15 min following KA injection and observed that $P2Y_1$ was already increased at this time in microglia (Fig. 6*A*). These findings are consistent with status epilepticus driving an early appearance of $P2Y_1$ in microglia that might influence their inflammatory state. To test whether microglial $P2Y_1$ receptor activity exerts a proinflammatory effect, we tested the effects of the broad-spectrum anti-inflammatory drug minocycline (30 mg/kg) in combination with targeting of $P2Y_1$ after KA injection (Fig. 6*B*). Minocycline treatment alone reduced hippocampal transcription of the microglia markers *Iba1* and fractalkine receptor *Cx3Cr1* (Fig. 6*C*) without affecting transcript levels of the astrocyte markers *GFAP* and *ALDH1L1* (Fig. 6*D*). This suggests that minocycline regulates microglia rather than astrocytes, confirming previous data suggesting minocycline blocking the proliferation of microglia (Abraham et al., 2012).

We then investigated the effect of delivering the $P2Y_1$ antagonist, MRS25, following the onset of seizures in mice pretreated with minocycline 24 h before KA. In contrast to naive mice, minocycline-pretreated mice showed an increased seizure severity when MRS25 was delivered at this time point (Fig. 6*E*,*F*). With early changes in $P2Y_1$ expression most evident on microglia, we wondered whether $P2Y_1$ antagonism interferes with cytokine release in the hippocampus. $P2Y_1$ antagonism reduced hippocampal concentrations of IL-1β during status epilepticus without altering concentrations of TNF-α (Fig. 6*G*), suggesting that $P2Y_1$ may drive microglial activation during status epilepticus. To further explore the effects of the $P2Y_1$ antagonist on microglia activation, microglia cells were isolated from brain tissue and treated with glutamate (100 μM) with and without the $P2Y_1$ antagonist MRS25 (10 μM). Further supporting a role of $P2Y_1$ in microglia regulation, our results show that $P2Y_1$ antagonism blocks the activation of microglia *in vitro* (Fig. 6*H*).

Together, these results suggest that the effects of $P2Y_1$ on seizure severity are partly mediated via driving microglial activation.

$P2Y_1$ antagonism delays the development of epilepsy following status epilepticus

To investigate the potential antiepileptogenic effect of $P2Y_1$ antagonism, a subset of mice were fitted with EEG telemetry units, which allows for continuous EEG recording (Moran et al., 2013).

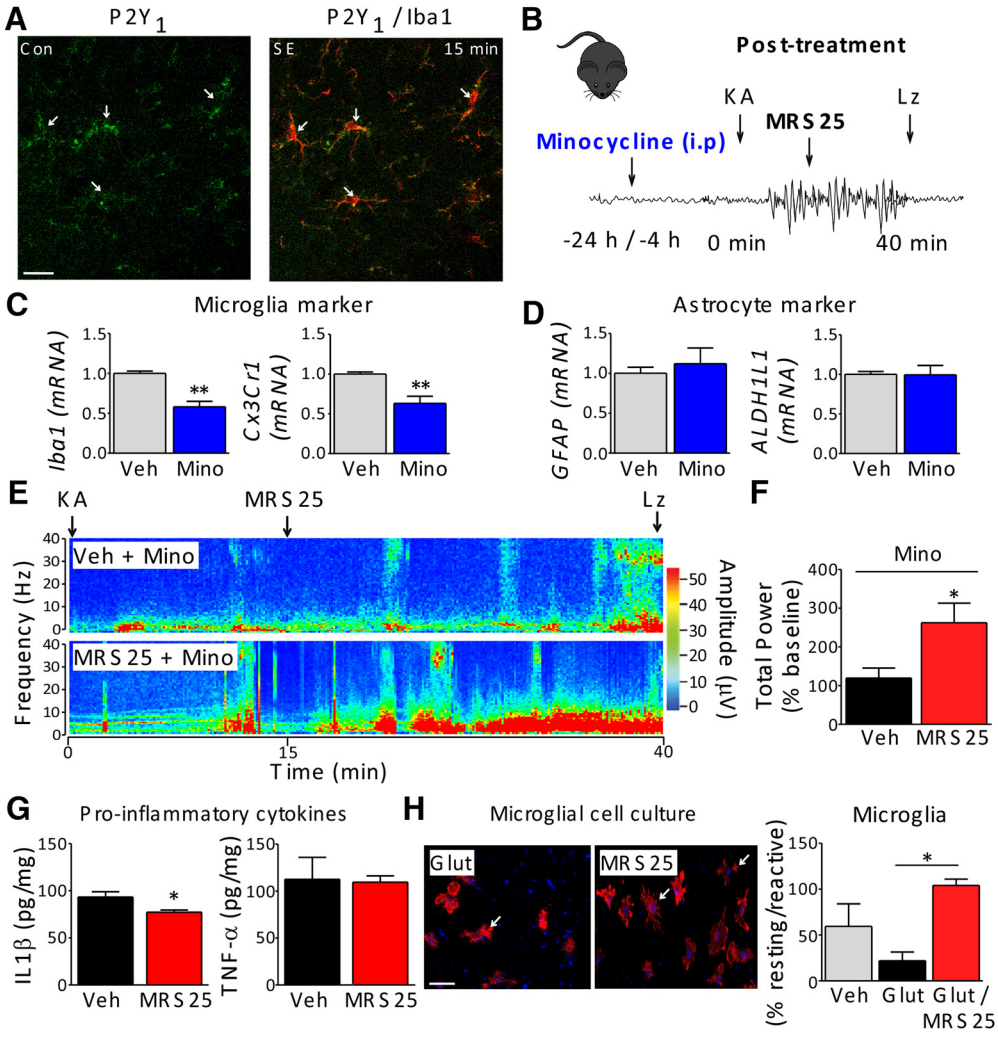

Figure 6. $P2Y_1$-driven microglia activation contributes to seizures during status epilepticus. ***A***, Photomicrographs showing colocalization of $P2Y_1$ (green) with the microglia marker Iba1 (red) in the CA3 region of the hippocampus 15 min after KA injection. Scale bar, 50 μm. ***B***, Schematic showing experimental design using the broad-spectrum inflammation blocker minocycline (Mino). Mice were treated with Mino (30 mg/kg, i.p.) 4 and 24 h before intra-amygdala KA-induced status epilepticus. $P2Y_1$ antagonist MRS25 was injected 15 min after KA. ***C***, Mino treatment leads to a reduction of hippocampal *Iba1* (1.000 ± 0.029 vs 0.5820 ± 0.0672, $t = 5.201$, df = 7, $p = 0.0013$, unpaired Student's *t* test) and *Cx3Cr1* (1.000 ± 0.0265 vs 0.6317 ± 0.0885, $t = 3.576$, df = 7, $p = 0.0090$, unpaired Student's *t* test) mRNA levels. ***D***, No difference was observed in hippocampal *GFAP* (1.003 ± 0.0749 vs 1.120 ± 0.1978, $t = 0.5027$, df = 7, $p = 0.63$, unpaired Student's *t* test) and *ALDH1L1* (1.000 ± 0.037 vs 0.9947 ± 0.1184, $t = 0.039$, df = 7, $p = 0.97$, unpaired Student's *t* test) mRNA levels ($n = 4$ Veh and $n = 5$ Mino). ***E***, Representative EEG recordings presented as heat maps of frequency and amplitude data during status epilepticus in mice treated with Mino and $P2Y_1$ antagonist MRS25 or Veh and Mino. ***F***, Graph showing a significant increase of total power and amplitude in mice treated with $P2Y_1$ antagonist MRS25 during status epilepticus in Mino-treated mice ($n = 4$ per group; unpaired Student's *t* test: total power: 119.5 ± 25.95 μV^2 vs 262.5 ± 50.85 μV^2, $t = 2.505$, df = 6, $p = 0.046$). ***G***, Graphs showing a reduction in the level of the proinflammatory cytokine IL-1β in mice treated with $P2Y_1$ antagonist MRS25. No difference was observed in the levels of TNF-α ($n = 4$ per group; unpaired Student's *t* test; IL-1β: 96.43 ± 5.414 pg/mg vs 77.34 ± 2.203 pg/mg, $t = 2.759$, df = 6, $p = 0.033$; TNF-α: 112.7 ± 23.32 pg/mg vs 109.0 ± 6.754 pg/mg, $t = 0.1548$, df = 6, $p = 0.88$). ***H***, Immunofluorescent staining (40× lens) and graph showing significant increase in the percentage of resting compared with reactive microglia when treated with the $P2Y_1$ antagonist MRS25 ($n = 3$ per group; one-way ANOVA with Fisher's *post hoc* test; Glut vs Glut-MRS25: 21.94 ± 9.526 vs 104.0 ± 6.894, $F = 6.788$, df = 2, $p = 0.010$). Scale bar, 50 μm. Data are mean ± SEM. *$p < 0.05$, **$p < 0.01$.

In order not to interfere with status epilepticus, mice were treated with the $P2Y_1$ antagonist MRS25 1 and 24 h after intra-amygdala KA-induced status epilepticus. Mice were then killed 14 d later (Fig. 7*A*).

First, to determine whether $P2Y_1$ antagonism impacts on inflammatory pathways during epileptogenesis, we analyzed transcription of the microglia markers, *Iba1* and *Cx3Cr1*, and astrocyte marker, *GFAP*, 24 h after status epilepticus. Mice treated with the $P2Y_1$ antagonist, MRS25, showed a significant reduction of *Iba1* and *Cx3Cr1* mRNA (Fig. 7*B*). No differences were observed in the mRNA levels of *GFAP* (Fig. 7*B*), further suggesting $P2Y_1$ driving microglial activation rather than astrocytosis following status epilepticus.

We then analyzed the occurrence of spontaneous seizures in both treatment groups. Treatment with the $P2Y_1$ antagonist MRS25 shortly after status epilepticus resulted in a later spontaneous seizure onset compared with Veh-injected mice (Fig. 7*C*). $P2Y_1$ antagonism thereby delays the emergence of epilepsy in the intra-amygdala KA model. Treatment with the $P2Y_1$ antagonist, MRS25, also slightly reduced the frequency of spontaneous seizures, with seizure frequency significantly lower in $P2Y_1$ antagonist-treated mice during the first recording week (Fig. 7*D*). Over the second week, seizure frequency in mice treated with the $P2Y_1$ antagonist MRS25 gradually recovered toward the Veh group (Fig. 7*D*). We also found that high-frequency high amplitude spiking (>60 s) was shorter in the $P2Y_1$ antagonist-treated

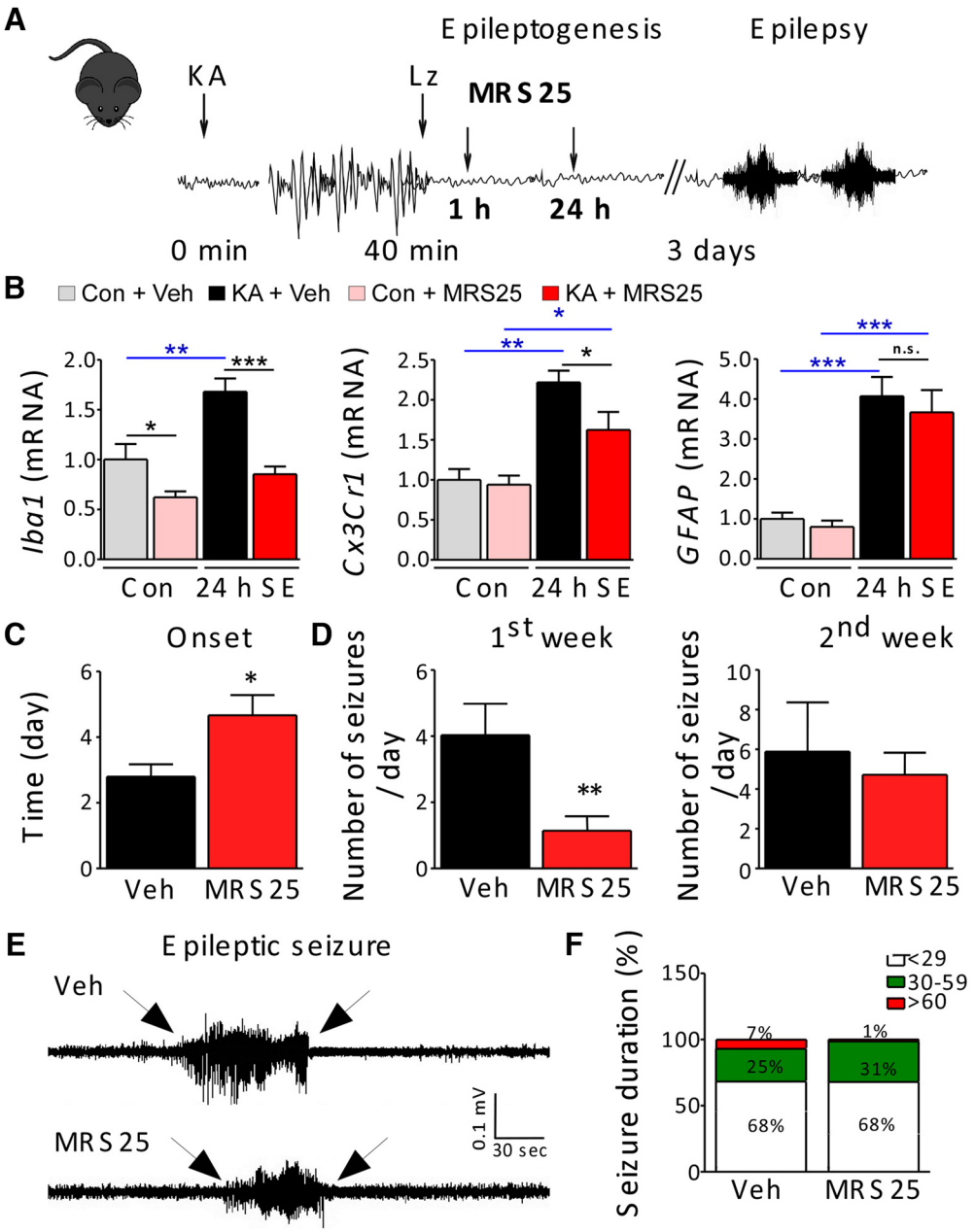

Figure 7. $P2Y_1$ receptor antagonism delays epileptogenesis. ***A***, Experimental design to investigate impact of $P2Y_1$ antagonism on epileptogenesis. $P2Y_1$ antagonist MRS25 was administered intracerebroventricularly 1 and 24 h following intra-amygdala KA. EEG was recorded for the following 14 d using EEG telemetry devices. ***B***, Graphs showing reduced levels of *Iba1* and *Cx3Cr1* mRNA and no changes in *GFAP* mRNA levels in $P2Y_1$ antagonist MRS25-treated mice 24 h after status epilepticus ($n = 4$ per group; one-way ANOVA with Fisher's *post hoc* test; *Iba1*: Con Veh vs Con MRS25: 1.003 ± 0.1541 vs 0.6225 ± 0.0596, $F = 16.21$, df = 3, $p = 0.035$; Con Veh vs 24 h SE Veh: 1.003 ± 0.1542 vs 1.680 ± 0.1339, $F = 16.21$, df = 3, $p = 0.0011$; 24 h SE Veh vs 24 h SE MRS25: 1.680 ± 0.1339 vs 0.8550 ± 0.076, $F = 16.21$, df = 3, $p = 0.0002$; *CX3Cr1*: Con Veh vs 24 h SE Veh: 1.000 ± 0.1369 vs 2.220 ± 0.1465, $F = 12.85$, df = 3, $p = 0.0002$; Con MRS25 vs 24 h SE MRS25: 0.9400 ± 0.1137 vs 1.625 ± 0.2239, $F = 12.85$, df = 3, $p = 0.019$; 24 h SE Veh vs 24 h SE MRS25: 2.220 ± 0.1465 vs 1.625 ± 0.2239, $F = 12.85$, df = 3, $p = 0.025$; *GFAP*: 24 h SE Veh vs 24 h SE MRS25: 4.073 ± 0.4791 vs 3.670 ± 0.5591, $F = 20.09$, df = 3, $p = 0.47$). ***C***, Graph showing a later seizure onset in mice treated with $P2Y_1$ antagonist MRS25 compared with Veh-injected mice ($n = 5$ Veh, and $n = 6$ MRS25; unpaired Student's *t* test: 2.800 ± 0.3742 min vs 4.667 ± 0.6146 min, $t = 2.460$, df = 9, $p = 0.036$). ***D***, Mice treated with the $P2Y_1$ antagonist MRS25 display significantly fewer seizures per day than Veh-injected mice during the first recording week (days 1–7; unpaired Student's *t* test: 20.75 ± 4.768 vs 4.333 ± 1.333, $t = 3.984$, df = 8, $p = 0.0040$). No significant change was observed during the second week (days 8–14; unpaired Student's *t* test: 34.00 ± 11.85 vs 32.00 ± 8.226, $t = 0.1438$, df = 8, $p = 0.89$; $n = 5$ Veh, and $n = 6$ MRS25). ***E***, Examples of epileptic seizures from Veh- and MRS25-treated mice during the 14 d recoding period (between arrows). ***F***, Graph showing percentage of average seizure duration of mice treated with Veh or the $P2Y_1$ antagonist MRS25 over the entire 14 d recording period following status epilepticus ($n = 5$ Veh, and $n = 6$ MRS25). Data are mean ± SEM. *$p < 0.05$, **$p < 0.01$, ***$p < 0.001$, n.s., non-significant.

group compared with the Veh-injected group (<29 s: Veh 68% vs MRS25 68%; 30–59 s: Veh 25% vs MRS25 31%; >60 s: Veh 7% vs MRS25 1%; Figure 7*E*,*F*).

Thus, our results suggest that early antagonism of the $P2Y_1$ receptor after status epilepticus delays the development of epilepsy and may produce a lasting disease-modifying action on seizure severity.

$P2Y_1$ antagonism suppresses occurrence of seizures during chronic epilepsy

Previous data published by us have also shown increased $P2Y_1$ expression in experimental epilepsy and in brain tissue obtained from patients who underwent resective surgery for drug-resistant temporal lobe epilepsy (Alves et al., 2017). To determine in which cell types $P2Y_1$ is upregulated in epilepsy, mice were killed 14 d

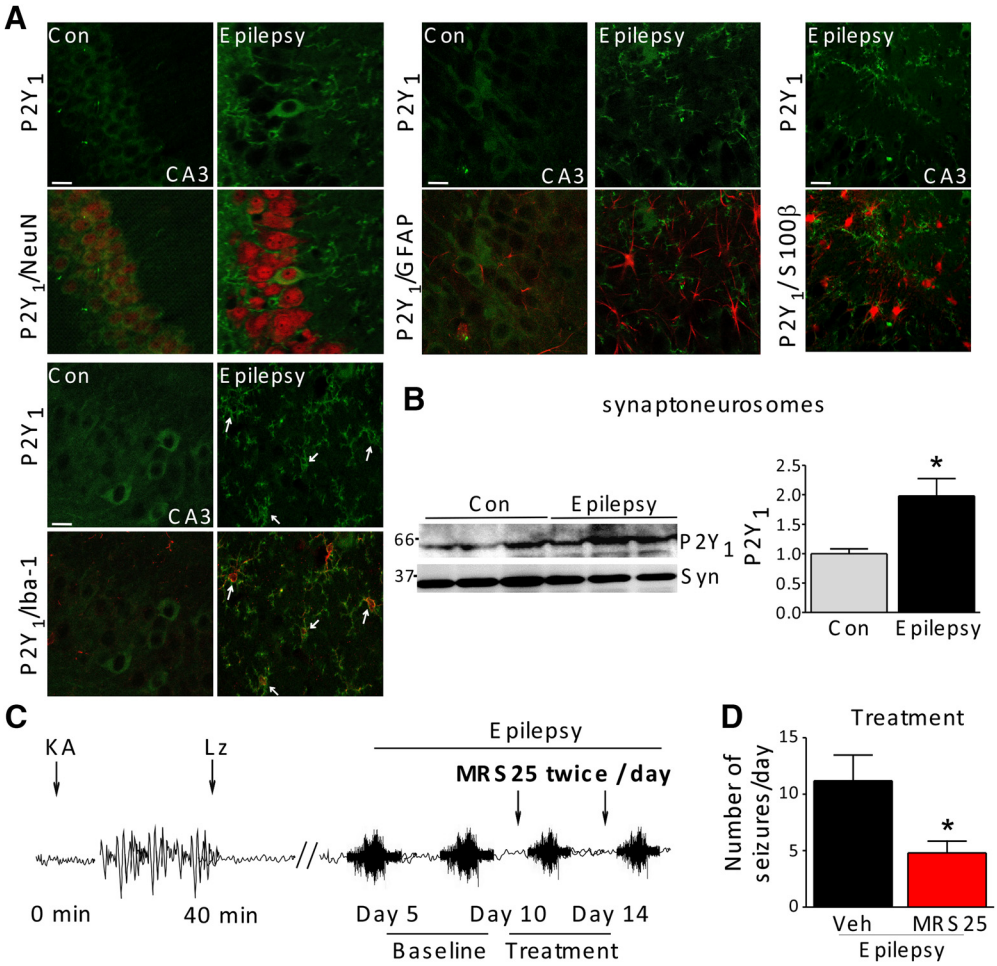

Figure 8. $P2Y_1$ antagonism during epilepsy suppresses spontaneous seizures. ***A***, Photomicrographs (40× lens) showing colocalization of $P2Y_1$ (green) with Iba1 (red) and NeuN (red) in the CA3 region of the hippocampus of epileptic mice at day 14 after status epilepticus. $P2Y_1$ did not colocalize with the astrocyte markers GFAP and S100β (red). White arrows indicate colocalization of $P2Y_1$ with microglia and neurons in the hippocampus. Scale bar, 50 μm. ***B***, Western blot ($n = 2$ hippocampi per lane) and representative graph showing a significant increase in $P2Y_1$ protein levels in synaptoneurosomes in epileptic mice: $n = 4$ (control [Con]) and 5 (epilepsy) (unpaired Student's t test: 1.000 ± 0.0848 vs 1.980 ± 0.2938, $t = 2.87$, df = 7, $p = 0.024$). ***C***, Experimental design to study effect of $P2Y_1$ antagonism during epilepsy. Epilepsy was induced via intra-amygdala KA and seizure baseline recorded from day 5–9. Mice were then treated with $P2Y_1$ antagonist MRS25 twice daily (1 nmol, i.c.v.) from day 10–14. This was followed by an additional 5 d recording during drug washout. ***D***, Mice treated with $P2Y_1$ antagonist MRS25 displayed significantly less seizures during treatment compared with Veh-injected mice ($n = 6$ per group; unpaired Student's t test: 11.20 ± 2.266 vs 4.808 ± 1.034, $t = 2.566$, df = 10, $p = 0.028$). Data are mean ± SEM. *$p < 0.05$.

after status epilepticus and brain sections analyzed by immunofluorescence, using markers for microglia (Iba1), neurons (NeuN), and astrocytes (GFAP, S100β). Immunostaining results showed that $P2Y_1$ is mainly expressed on neurons and microglia (Fig. 8*A*). No staining was evident on astrocytes (Fig. 8*A*). Further, $P2Y_1$ was also significantly increased in hippocampal synaptoneurosomes during epilepsy (Fig. 8*B*). Thus, our results show, similar to status epilepticus, a mainly neuronal and microglial expression of $P2Y_1$ during chronic epilepsy.

To explore whether $P2Y_1$ antagonism suppresses the occurrence of spontaneous seizures, mice were treated with the $P2Y_1$ antagonist MRS25 (1 nmol) or Veh intracerebroventricularly twice daily from day 10 to day 14, followed by a 5 d washout period (Fig. 8*C*). All mice in this study experienced at least one seizure at day 3 after status epilepticus. No difference was observed in seizure frequency during baseline recording between treatment groups (7.3 ± 2.8 Veh and 5.2 ± 2.3 MRS25, $p = 0.48$; unpaired t test). Treatment with the $P2Y_1$ antagonist MRS25 reduced seizure frequency by 43% during treatment (Fig. 8*D*). Seizure frequency in the $P2Y_1$ antagonist-treated group, however, returned to Veh-treated levels during washout period (8.7 ± 2.2 Veh vs 10.7 ± 3.1 MRS25, $p = 0.60$). To test whether $P2Y_1$ antagonism had any effects on seizure duration, individual seizures were analyzed. No significant difference was observed between $P2Y_1$ antagonist-treated mice compared with the Veh-injected group during treatment (<29 s: Veh 43% vs MRS25 20%; 30–59 s: Veh 33% vs MRS25 66%, >60 s: Veh 24% vs MRS25 5%).

Together, our results show seizure-suppressive potential of $P2Y_1$ antagonism during epilepsy, suggesting that $P2Y_1$-targeting drugs may be effective in drug-refractory epilepsy.

Discussion

Here, we demonstrate that $P2Y_1$ activation has a unique and remarkable dual effect on seizures and seizure-induced pathology according to the time point of $P2Y_1$ stimulation. We show that $P2Y_1$, when activated before status epilepticus, protects the brain from seizures and damage. However, when activated once status epilepticus had been triggered or during epilepsy, $P2Y_1$ acts as proconvulsant, possibly via the activation of microglia.

In our first findings, we show that, under physiological condition, $P2Y_1$ is expressed in neurons in agreement with other previous studies (Moore et al., 2000). Although we did not focus on the specific expression pattern within neurons, previous work showed that $P2Y_1$ is expressed in the soma and mossy fiber terminals of the CA3 subfield of the hippocampus (Csölle et al., 2008). This would be consistent with a physiological function in reducing neurotransmitter release. In contrast to other studies (Fischer et al., 2009), we did not observe $P2Y_1$ under baseline conditions in either microglia or astrocytes in the mouse hippocampus. Status epilepticus caused a strong upregulation of $P2Y_1$ in neurons but also in microglia. This fits with previous studies showing microglia upregulating $P2Y_1$ following TGF-β addition (De Simone et al., 2010). As observed under physiological conditions, $P2Y_1$ was not expressed by astrocytes. This contrasts with other reports that observed $P2Y_1$ expression on astrocytes under different pathological conditions, including oxidative stress (Shinozaki et al., 2006; Fujita et al., 2009) and ischemia (Zheng et al., 2013). Of note, where astrocyte expression has been reported, this has been linked with protective effects. For example, overactivation of $P2Y_1$ was reported to prevent damage in astrocytes caused by oxidative stress (Shinozaki et al., 2006) or prevent neuronal damage through IL-6 release (Fujita et al., 2009). Also, treatment with the $P2Y_1$ agonist 2-MeSADP reduced cytotoxic edema and ischemic lesions through enhanced astrocyte mitochondrial metabolism due to increased inositol trisphosphate-dependent Ca^{2+} release (Zheng et al., 2013). It is unclear why we did not find $P2Y_1$ expressed on astrocytes. In our studies, we included specificity controls and demonstrated loss of $P2Y_1$ staining in $P2Y_1^{-/-}$ tissue as a negative control. $P2Y_1$ expression may also increase according to insult in a cell-specific manner.

One of the main and most remarkable findings here is that manipulation of $P2Y_1$ causes bidirectional exacerbation of seizure severity according to when the manipulation was performed. We found that activating $P2Y_1$ before induction of status epilepticus reduced seizures and protected the hippocampus. This finding is consistent with a role for $P2Y_1$ in reducing excessive excitation in the brain. Notably, $P2Y_1$ is found presynaptically where it may function to increase synaptic inhibition (Bowser and Khakh, 2004; Kawamura et al., 2004) or attenuate neurotransmitter release (e.g., glutamate) (Mendoza-Fernández et al., 2000; Rodrigues et al., 2005). In addition to the pharmacologic approaches used to interrogate the function of $P2Y_1$, we explored the effects of status epilepticus in $P2Y_1$-deficient mice. A strong susceptibility to seizures was observed in $P2Y_1^{-/-}$ mice, which can be explained by the high levels of the kainate receptor GLUR6/7, which may aggravate the seizure phenotype (Crépel and Mulle, 2015). Notably, mice heterozygous for $P2Y_1$ experienced a similar increase in seizure severity as observed for $P2Y_1^{-/-}$ mice, indicating that loss of a single copy of $P2Y_1$ is sufficient to enhance brain excitability. These results suggest that even minor changes to $P2Y_1$ function may impact on seizure susceptibility and further stress the likely functional consequences of any changes to $P2Y_1$ levels in epilepsy. In line with our study, ADP-sensitive $P2Y_{12}$-deficient mice also showed an exacerbated seizure phenotype (Eyo et al., 2014).

$P2Y_1$ activation after the induction of status epilepticus potentiated the generation of seizures. We have shown that following status epilepticus, $P2Y_1$ is also expressed on microglia, suggesting a role of $P2Y_1$ on microglial activation and possibly in driving inflammation. Indeed, during brain inflammation, microglia are the first cells to respond (Davalos et al., 2005; Eyo et al., 2014). Microglia also respond rapidly to brain injury and acute neuronal hyperactivity during seizures through NMDA-type glutamate receptors (Davalos et al., 2005; Eyo et al., 2014). A role for purinergic receptors, including $P2Y_1$, on microglial function is well established (Färber and Kettenmann, 2006). $P2Y_1$ functions on microglia to mediate microglial migration (Davalos et al., 2005; De Simone et al., 2010). In contrast to our study, which suggests $P2Y_1$-driven microglial activation being detrimental during status epilepticus, a recent study showed that $P2Y_1$ expressed on microglia was protective against ischemia (Fukumoto et al., 2018), suggesting that the contribution of $P2Y_1$ expressed on microglia is disease-specific. Another study showed that activated microglia can drive the transformation of astrocytes toward a neuroprotective phenotype, through downregulation of astrocyte-expressed $P2Y_1$ (Shinozaki et al., 2017). We cannot exclude a functional contribution for astrocytic $P2Y_1$ in our model. To prove this would, however, require the use of cell-specific $P2Y_1$-deficient mice in the future.

Another important aspect of our study was to show that the core findings in the KA model were reproduced in the pilocarpine model. This avoids a common concern that an observation is unique to a particular model. Because no single model represents all aspects of the condition, it is important to replicate key findings. Here we show that the pretreatment and post-treatment consequences of $P2Y_1$ modulation are similar in the pilocarpine model. Notably, other studies that investigated P2 family members in epilepsy only looked at single models (Eyo et al., 2014; Simoes et al., 2018) or even found contradictory results, such as reported for P2X7 (Kim and Kang, 2011; Engel et al., 2012).

Status epilepticus is known to elicit irreversible brain damage in both experimental models and humans (Betjemann and Lowenstein, 2015). Here we found that blocking $P2Y_1$ after status epilepticus induction reduced seizure severity and protected the brain from damage. However, $P2Y_1$ activation after status epilepticus, despite increasing seizure severity, did not cause more neuronal damage, suggesting $P2Y_1$-mediated neuroprotective effects. This is also in line with our *in vitro* results, where we demonstrated that $P2Y_1$ overexpression protected against KA-induced neuronal death. However, our results are in contrast to studies showing that $P2Y_1$ antagonism protects from glutamate-induced excitotoxicity *in vivo* and *in vitro* (Choo et al., 2013; Simoes et al., 2018). Possible explanations for this discrepancy include the use of a different species (mouse vs rat), differences in how status epilepticus was triggered (intra-amygdala vs systemic), or excitotoxic agent used (KA vs glutamate). Of note, $P2Y_1^{-/-}$ mice, despite experiencing a more severe phenotype during status epilepticus resulting in more FjB-positive cells, showed also a reduction in astrocytes. This is in line with previous studies demonstrating $P2Y_1$ driving astrocyte activation (Delekate et al., 2014; Álvarez-Ferradas et al., 2015).

We also observed a delayed onset of spontaneous seizures and a reduction in seizure duration in mice treated with the $P2Y_1$ antagonist MRS25 following status epilepticus. In line with microglia and not astrocytes driving $P2Y_1$-induced pathology during epileptogenesis, mice treated with MRS25 had a strong decrease in the microglia marker *Iba1* and *Cx3Cr1* but not in the astrocyte marker *GFAP* during the latent period. Thus, reduction of microglia activation in the latent period caused by $P2Y_1$ antagonism may contribute to delaying the occurrence of the first spontaneous seizure. An alternative explanation for the antiepileptogenic effect provided by $P2Y_1$ antagonism are possible effects of $P2Y_1$ on aberrant neurogenesis; $P2Y_1$ has been found to be increased on neuronal progenitor cells following status epilepticus (Rozmer et al., 2017), and aberrant neurogenesis has been

shown to alter the development of epilepsy (Cho et al., 2015). The observed antiepileptogenic effects, however, were decreasing over the second week, suggesting that $P2Y_1$-mediated effects on epileptogenesis are not long-lasting. Nevertheless, our study is the first demonstrating a functional role of any P2Y receptor on epileptogenesis *in vivo*, suggesting that targeting this class of receptors may provide antiepileptogenic effects possibly via reducing inflammation.

The last finding in our study was a strong seizure-suppressive effect of $P2Y_1$ antagonism during chronic epilepsy. We have not analyzed the mechanism of how $P2Y_1$ antagonism reduces seizures during epilepsy; however, the strong immunoreactivity of $P2Y_1$ on microglia suggests this via $P2Y_1$-mediated activation of microglia. Data demonstrating a role for inflammation during epileptogenesis showed that the inhibition of upstream Toll-like receptor signaling reduces spontaneous seizures and brain inflammation (Maroso et al., 2010, 2011). Further, brain tissue from epileptic mice and epileptic patients presents high levels of proinflammatory cytokines (Aronica et al., 2017), and blocking these cytokines has been implicated in the reduction of seizures during chronic epilepsy (Ravizza et al., 2008). Following treatment, seizure numbers in $P2Y_1$ antagonist-treated mice, however, increased again to baseline levels. This suggests that effects provided by $P2Y_1$ antagonism are rather anticonvulsive than disease-modifying. Regardless of the lack of disease-modifying effects, this is the first study showing a seizure-suppressive effect resulting from the inhibition of the $P2Y_1$ receptor in drug-refractory chronic epilepsy.

In conclusion, our study found potent seizure-suppressive effects of $P2Y_1$ antagonism during status epilepticus, epileptogenesis, and chronic epilepsy, suggesting that $P2Y_1$ receptor antagonists may be a novel candidate for the treatment of drug-refractory status epilepticus and epilepsy.

References

Abraham J, Fox PD, Condello C, Bartolini A, Koh S (2012) Minocycline attenuates microglia activation and blocks the long-term epileptogenic effects of early-life seizures. Neurobiol Dis 46:425–430.

Álvarez-Ferradas C, Morales JC, Wellmann M, Nualart F, Roncagliolo M, Fuenzalida M, Bonansco C (2015) Enhanced astroglial Ca^{2+} signaling increases excitatory synaptic strength in the epileptic brain. Glia 63: 1507–1521.

Alves M, Gomez-Villafuertes R, Delanty N, Farrell MA, O'Brien DF, Miras-Portugal MT, Hernandez MD, Henshall DC, Engel T (2017) Expression and function of the metabotropic purinergic P2Y receptor family in experimental seizure models and patients with drug-refractory epilepsy. Epilepsia 58:1603–1614.

Alves M, Beamer E, Engel T (2018) The metabotropic purinergic P2Y receptor family as novel drug target in epilepsy. Front Pharmacol 9:193.

Aronica E, Bauer S, Bozzi Y, Caleo M, Dingledine R, Gorter JA, Henshall DC, Kaufer D, Koh S, Loscher W, Louboutin JP, Mishto M, Norwood BA, Palma E, Poulter MO, Terrone G, Vezzani A, Kaminski RM (2017) Neuroinflammatory targets and treatments for epilepsy validated in experimental models. Epilepsia 58 [Suppl 3]:27–38.

Beamer E, Fischer W, Engel T (2017) The ATP-gated P2X7 receptor as a target for the treatment of drug-resistant epilepsy. Front Neurosci 11:21.

Betjemann JP, Lowenstein DH (2015) Status epilepticus in adults. Lancet Neurol 14:615–624.

Bowser DN, Khakh BS (2004) ATP excites interneurons and astrocytes to increase synaptic inhibition in neuronal networks. J Neurosci 24:8606–8620.

Brennan GP, Jimenez-Mateos EM, McKiernan RC, Engel T, Tzivion G, Henshall DC (2013) Transgenic overexpression of 14–3-3 zeta protects hippocampus against endoplasmic reticulum stress and status epilepticus in vivo. PLoS One 8:e54491.

Burnstock G (2007) Physiology and pathophysiology of purinergic neurotransmission. Physiol Rev 87:659–797.

Burnstock G (2013) Introduction to purinergic signalling in the brain. Adv Exp Med Biol 986:1–12.

Burnstock G, Knight GE (2004) Cellular distribution and functions of P2 receptor subtypes in different systems. Int Rev Cytol 240:31–304.

Carmo MR, Simões AP, Fonteles AA, Souza CM, Cunha RA, Andrade GM (2014) ATP P2Y1 receptors control cognitive deficits and neurotoxicity but not glial modifications induced by brain ischemia in mice. Eur J Neurosci 39:614–622.

Choo AM, Miller WJ, Chen YC, Nibley P, Patel TP, Goletiani C, Morrison B 3rd, Kutzing MK, Firestein BL, Sul JY, Haydon PG, Meaney DF (2013) Antagonism of purinergic signalling improves recovery from traumatic brain injury. Brain 136:65–80.

Cho KO, Lybrand ZR, Ito N, Brulet R, Tafacory F, Zhang L, Good L, Ure K, Kernie SG, Birnbaum SG, Scharfman HE, Eisch AJ, Hsieh J (2015) Aberrant hippocampal neurogenesis contributes to epilepsy and associated cognitive decline. Nat Commun 6:6606.

Crépel V, Mulle C (2015) Physiopathology of kainate receptors in epilepsy. Curr Opin Pharmacol 20:83–88.

Csölle C, Heinrich A, Kittel A, Sperlágh B (2008) P2Y receptor mediated inhibitory modulation of noradrenaline release in response to electrical field stimulation and ischemic conditions in superfused rat hippocampus slices. J Neurochem 106:347–360.

Curia G, Longo D, Biagini G, Jones RS, Avoli M (2008) The pilocarpine model of temporal lobe epilepsy. J Neurosci Methods 172:143–157.

Dale N, Frenguelli BG (2009) Release of adenosine and ATP during ischemia and epilepsy. Curr Neuropharmacol 7:160–179.

Davalos D, Grutzendler J, Yang G, Kim JV, Zuo Y, Jung S, Littman DR, Dustin ML, Gan WB (2005) ATP mediates rapid microglial response to local brain injury in vivo. Nat Neurosci 8:752–758.

De Simone R, Niturad CE, De Nuccio C, Ajmone-Cat MA, Visentin S, Minghetti L (2010) TGF-beta and LPS modulate ADP-induced migration of microglial cells through P2Y1 and P2Y12 receptor expression. J Neurochem 115:450–459.

Delekate A, Füchtemeier M, Schumacher T, Ulbrich C, Foddis M, Petzold GC (2014) Metabotropic P2Y1 receptor signalling mediates astrocytic hyperactivity in vivo in an Alzheimer's disease mouse model. Nat Commun 5:5422.

Engel T, Gomez-Villafuertes R, Tanaka K, Mesuret G, Sanz-Rodriguez A, Garcia-Huerta P, Miras-Portugal MT, Henshall DC, Diaz-Hernandez M (2012) Seizure suppression and neuroprotection by targeting the purinergic P2X7 receptor during status epilepticus in mice. FASEB J 26: 1616–1628.

Engel T, Sanz-Rodgriguez A, Jimenez-Mateos EM, Concannon CG, Jimenez-Pacheco A, Moran C, Mesuret G, Petit E, Delanty N, Farrell MA, O'Brien DF, Prehn JH, Lucas JJ, Henshall DC (2013) CHOP regulates the p53-MDM2 axis and is required for neuronal survival after seizures. Brain 136:577–592.

Engel T, Alves M, Sheedy C, Henshall DC (2016) ATPergic signalling during seizures and epilepsy. Neuropharmacology 104:140–153.

Engel T, Brennan GP, Sanz-Rodriguez A, Alves M, Beamer E, Watters O, Henshall DC, Jimenez-Mateos EM (2017a) A calcium-sensitive feed-forward loop regulating the expression of the ATP-gated purinergic P2X7 receptor via specificity protein 1 and microRNA-22. Biochim Biophys Acta Mol Cell Res 1864:255–266.

Engel T, Martinez-Villarreal J, Henke C, Jimenez-Mateos EM, Sanz-Rodriguez A, Alves M, Hernandez-Santana Y, Brennan GP, Kenny A, Campbell A, Lucas JJ, Henshall DC (2017b) Spatiotemporal progression of ubiquitin-proteasome system inhibition after status epilepticus suggests protective adaptation against hippocampal injury. Mol Neurodegener 12:21.

Engel T, Gómez-Sintes R, Alves M, Jimenez-Mateos EM, Fernández-Nogales M, Sanz-Rodriguez A, Morgan J, Beamer E, Rodríguez-Matellán A, Dunleavy M, Sano T, Avila J, Medina M, Hernandez F, Lucas JJ, Henshall DC (2018) Bi-directional genetic modulation of GSK-3beta exacerbates hippocampal neuropathology in experimental status epilepticus. Cell Death Dis 9:969.

Eyo UB, Peng J, Swiatkowski P, Mukherjee A, Bispo A, Wu LJ (2014) Neuronal hyperactivity recruits microglial processes via neuronal NMDA receptors and microglial P2Y12 receptors after status epilepticus. J Neurosci 34:10528–10540.

Färber K, Kettenmann H (2006) Purinergic signaling and microglia. Pflugers Arch 452:615–621.

Fischer W, Appelt K, Grohmann M, Franke H, Nörenberg W, Illes P (2009) Increase of intracellular Ca^{2+} by P2X and P2Y receptor-subtypes in cultured cortical astroglia of the rat. Neuroscience 160:767–783.

Fujita T, Tozaki-Saitoh H, Inoue K (2009) P2Y1 receptor signaling enhances neuroprotection by astrocytes against oxidative stress via IL-6 release in hippocampal cultures. Glia 57:244–257.

Fukumoto Y, Tanaka KF, Parajuli B, Shibata K, Yoshioka H, Kanemaru K, Gachet C, Ikenaka K, Koizumi S, Kinouchi H (2018) Neuroprotective effects of microglial P2Y1 receptors against ischemic neuronal injury. J Cereb Blood Flow Metab. Advance online publication. Retrieved October 18, 2018. doi: 10.1177/0271678X18805317.

Guzman SJ, Gerevich Z (2016) P2Y receptors in synaptic transmission and plasticity: therapeutic potential in cognitive dysfunction. Neural Plast 2016:1207393.

Henshall DC, Engel T (2015) P2X purinoceptors as a link between hyperexcitability and neuroinflammation in status epilepticus. Epilepsy Behav 49:8–12.

Idzko M, Ferrari D, Riegel AK, Eltzschig HK (2014) Extracellular nucleotide and nucleoside signaling in vascular and blood disease. Blood 124:1029–1037.

Jimenez-Mateos EM, Arribas-Blazquez M, Sanz-Rodriguez A, Concannon C, Olivos-Ore LA, Reschke CR, Mooney CM, Mooney C, Lugara E, Morgan J, Langa E, Jimenez-Pacheco A, Silva LF, Mesuret G, Boison D, Miras-Portugal MT, Letavic M, Artalejo AR, Bhattacharya A, Diaz-Hernandez M, et al. (2015) microRNA targeting of the P2X7 purinoceptor opposes a contralateral epileptogenic focus in the hippocampus. Sci Rep 5:17486.

Jimenez-Pacheco A, Diaz-Hernandez M, Arribas-Blázquez M, Sanz-Rodriguez A, Olivos-Oré LA, Artalejo AR, Alves M, Letavic M, Miras-Portugal MT, Conroy RM, Delanty N, Farrell MA, O'Brien DF, Bhattacharya A, Engel T, Henshall DC (2016) Transient P2X7 receptor antagonism produces lasting reductions in spontaneous seizures and gliosis in experimental temporal lobe epilepsy. J Neurosci 36:5920–5932.

Kawamura M, Gachet C, Inoue K, Kato F (2004) Direct excitation of inhibitory interneurons by extracellular ATP mediated by P2Y1 receptors in the hippocampal slice. J Neurosci 24:10835–10845.

Kim JE, Kang TC (2011) The P2X7 receptor-pannexin-1 complex decreases muscarinic acetylcholine receptor-mediated seizure susceptibility in mice. J Clin Invest 121:2037–2047.

Kuboyama K, Harada H, Tozaki-Saitoh H, Tsuda M, Ushijima K, Inoue K (2011) Astrocytic P2Y(1) receptor is involved in the regulation of cytokine/chemokine transcription and cerebral damage in a rat model of cerebral ischemia. J Cereb Blood Flow Metab 31:1930–1941.

Maroso M, Balosso S, Ravizza T, Liu J, Aronica E, Iyer AM, Rossetti C, Molteni M, Casalgrandi M, Manfredi AA, Bianchi ME, Vezzani A (2010) Toll-like receptor 4 and high-mobility group box-1 are involved in ictogenesis and can be targeted to reduce seizures. Nat Med 16:413–419.

Maroso M, Balosso S, Ravizza T, Iori V, Wright CI, French J, Vezzani A (2011) Interleukin-1beta biosynthesis inhibition reduces acute seizures and drug resistant chronic epileptic activity in mice. Neurotherapeutics 8:304–315.

Mendoza-Fernández V, Andrew RD, Barajas-López C (2000) ATP inhibits glutamate synaptic release by acting at P2Y receptors in pyramidal neurons of hippocampal slices. J Pharmacol Exp Ther 293:172–179.

Moore D, Chambers J, Waldvogel H, Faull R, Emson P (2000) Regional and cellular distribution of the P2Y(1) purinergic receptor in the human brain: striking neuronal localisation. J Comp Neurol 421:374–384.

Moran C, Sanz-Rodriguez A, Jimenez-Pacheco A, Martinez-Villareal J, McKiernan RC, Jimenez-Mateos EM, Mooney C, Woods I, Prehn JH, Henshall DC, Engel T (2013) Bmf upregulation through the AMP-activated protein kinase pathway may protect the brain from seizure-induced cell death. Cell Death Dis 4:e606.

Mouri G, Jimenez-Mateos E, Engel T, Dunleavy M, Hatazaki S, Paucard A, Matsushima S, Taki W, Henshall DC (2008) Unilateral hippocampal CA3-predominant damage and short latency epileptogenesis after intra-amygdala microinjection of kainic acid in mice. Brain Res 1213:140–151.

Nikolic L, Shen W, Nobili P, Virenque A, Ulmann L, Audinat E (2018) Blocking TNFα-driven astrocyte purinergic signaling restores normal synaptic activity during epileptogenesis. Glia 66:2673–2683.

Ravizza T, Gagliardi B, Noé F, Boer K, Aronica E, Vezzani A (2008) Innate and adaptive immunity during epileptogenesis and spontaneous seizures: evidence from experimental models and human temporal lobe epilepsy. Neurobiol Dis 29:142–160.

Rodrigues RJ, Almeida T, Richardson PJ, Oliveira CR, Cunha RA (2005) Dual presynaptic control by ATP of glutamate release via facilitatory P2X1, P2X2/3, and P2X3 and inhibitory P2Y1, P2Y2, and/or P2Y4 receptors in the rat hippocampus. J Neurosci 25:6286–6295.

Rozmer K, Gao P, Araújo MGL, Khan MT, Liu J, Rong W, Tang Y, Franke H, Krügel U, Fernandes MJS, Illes P (2017) Pilocarpine-induced status epilepticus increases the sensitivity of P2X7 and P2Y1 receptors to nucleotides at neural progenitor cells of the juvenile rodent hippocampus. Cereb Cortex 27:3568–3585.

Shinozaki Y, Koizumi S, Ohno Y, Nagao T, Inoue K (2006) Extracellular ATP counteracts the ERK1/2-mediated death-promoting signaling cascades in astrocytes. Glia 54:606–618.

Shinozaki Y, Shibata K, Yoshida K, Shigetomi E, Gachet C, Ikenaka K, Tanaka KF, Koizumi S (2017) Transformation of astrocytes to a neuroprotective phenotype by microglia via P2Y1 receptor downregulation. Cell Rep 19:1151–1164.

Simões AP, Silva CG, Marques JM, Pochmann D, Porciúncula LO, Ferreira S, Oses JP, Beleza RO, Real JI, Köfalvi A, Bahr BA, Lerma J, Cunha RA, Rodrigues RJ (2018) Glutamate-induced and NMDA receptor-mediated neurodegeneration entails P2Y1 receptor activation. Cell Death Dis 9:297.

Talley Watts L, Sprague S, Zheng W, Garling RJ, Jimenez D, Digicaylioglu M, Lechleiter J (2013) Purinergic 2Y1 receptor stimulation decreases cerebral edema and reactive gliosis in a traumatic brain injury model. J Neurotrauma 30:55–66.

Vezzani A, Viviani B (2015) Neuromodulatory properties of inflammatory cytokines and their impact on neuronal excitability. Neuropharmacology 96:70–82.

von Kügelgen I, Hoffmann K (2016) Pharmacology and structure of P2Y receptors. Neuropharmacology 104:50–61.

Webb TE, Simon J, Barnard EA (1998) Regional distribution of [35S]2′-deoxy 5′-O-(1-thio) ATP binding sites and the P2Y1 messenger RNA within the chick brain. Neuroscience 84:825–837.

Zheng W, Talley Watts L, Holstein DM, Wewer J, Lechleiter JD (2013) P2Y1R-initiated, IP3R-dependent stimulation of astrocyte mitochondrial metabolism reduces and partially reverses ischemic neuronal damage in mouse. J Cereb Blood Flow Metab 33:600–611.